

Master thesis

**Polarization Measurements of  $\gamma$ -Rays  
in Mass  $A \sim 60$  Nuclei**

By Olga Izotova

Department of Physics  
Division of Nuclear Physics  
Lund University, 2003

**Abstract**

The polarization of  $\gamma$ -rays in various residual nuclei in the  $A=60$  region was measured using data from an EUROBALL experiment. The fusion-evaporation reaction  $^{24}\text{Mg}+^{40}\text{Ca}$  formed the compound nucleus  $^{64}\text{Ge}$ , which then decayed by emission of  $\alpha$ -particles, protons, neutrons and finally  $\gamma$ -rays. The polarization of  $\gamma$ -rays from the decay was measured and spins and parities for a number of states in various nuclei were deduced. It was especially important to identify parity changing E1 transitions. In the  $A=60$  mass region these E1 transitions pin down the influence of the positive-parity  $1g_{9/2}$  intruder orbital in the “sea” of states generated by excitations within the  $fp$  shell.

---

# Contents

<b>1. Theory</b>	<b>3</b>
1.1. History	3
1.2. Polarization of light	3
1.3. Polarization of $\gamma$ -rays	7
<b>2. Experimental methods</b>	<b>9</b>
2.1. The experiment	9
2.2. Fusion-evaporation reaction	10
2.3. Detectors	12
2.4. EUROBALL detection system	14
<b>3. Data analysis</b>	<b>15</b>
3.1. Identification of $\gamma$ -ray spectra	15
3.2. $\gamma$ - $\gamma$ coincidence matrix	16
3.3. Collection of statistics	18
3.4. Measurement of $\gamma$ -ray intensity	19
3.5. Normalization of the spectra and DCO-ratios	21
<b>4. Results</b>	<b>23</b>
<b>5. Discussion</b>	<b>31</b>
<b>Acknowledgments</b>	<b>37</b>
<b>References</b>	<b>38</b>

# 1 Theory

Light is a very complex phenomenon. Sometimes it acts like an electromagnetic wave, sometimes like small particles, photons. In this section I will describe the electromagnetic properties of light, and in particular its property polarization. This work focuses on the polarization of  $\gamma$ -rays.

## 1.1 History

The characteristics of light have been studied for a long time. The diffraction and interference phenomena provide evidence that light has wave nature. In the beginning it was believed that light was longitudinal waves due to its ability to pass through matter. The phenomenon of light polarization was known already in the days of Newton and Huygens. In 1669 Erasmus Bartholinus, doctor of medicine and professor of mathematics at the University of Copenhagen came upon a new and remarkable optical phenomenon in calcite or calcium carbonate ( $\text{CaCO}_3$ ), which he called double diffraction. He looked at a small object through a calcite crystal and discovered two refracted images. Some rays, which he called ordinary rays continued undeviated, and other rays, which he called extra ordinary rays traveled at some angle to the surface. If the rays passed from one crystal trough another the ordinary rays could turn into the extraordinary rays by rotating the second crystal relative to the first and vice versa. Two rays propagated at different speeds. This phenomenon could not be explained with longitudinal wave theory. Newton suggested that the light had "sides", like the poles of a magnet. The light would propagate either as ordinary or extra ordinary waves depending on how they were oriented to the structure of the crystal. This "sidedness" of light was later called **polarization** as a result of Newton's reference to magnets.

The work of J.C. Maxwell and subsequent developments since the late 1800s have made it evident that light is most certainly electromagnetic in nature and may be treated as transverse electromagnetic waves.

## 1.2 Polarization of light

A basic feature of Maxwell's equations for the electromagnetic field is the existence of traveling wave solutions, which represent the transport of energy from one point to another. In free space, far from the source of the fields, the fields satisfy Maxwell's wave equations [1]:

$$\frac{\partial^2 \mathbf{E}}{\partial z^2} = \mu_0 \epsilon_0 \frac{\partial^2 \mathbf{E}}{\partial t^2}$$

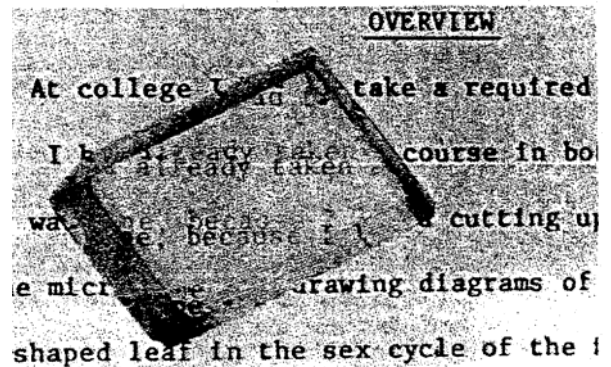


Figure 1.1. Two images produced by a doubly refracting or birefringent crystal. Taken from Ref. [1].

$$\frac{\partial^2 \mathbf{B}}{\partial z^2} = \mu_0 \varepsilon_0 \frac{\partial^2 \mathbf{B}}{\partial t^2},$$

where  $\mathbf{E}$  and  $\mathbf{B}$  are electric and magnetic fields vectors respectively.  $\mu_0$  and  $\varepsilon_0$  are permeability and permittivity constants in vacuum, and  $z$  is points coordinate on  $z$ -axis at the time  $t$ .

With the convention that the physical electric and magnetic fields are obtained by taking the real part of the complex quantities the simplest wave solutions are:

$$\mathbf{E}(\hat{z}, t) = \mathbf{i}E_0 \cos(k \cdot z - \omega t) \quad (1)$$

$$\mathbf{B}(\hat{z}, t) = \mathbf{j}B_0 \cos(k \cdot z - \omega t) \quad (2)$$

where  $\mathbf{i}$  and  $\mathbf{j}$  are the constant unit vectors (and not necessarily in  $x$ - and  $y$ -axis directions),  $E_0$  and  $B_0$  are the amplitudes, which are constant in space and time,  $k$  is the magnitude of the direction of propagation vector  $\mathbf{k}$  and  $\omega$  is the angular frequency. The magnitude of the wave vector  $\mathbf{k}$  and the frequency  $\omega$  are related by  $k = \frac{\omega}{v} = \sqrt{\mu\varepsilon} \frac{\omega}{c}$ , where  $\mu$  and  $\varepsilon$  are the permeability and permittivity parameters, respectively, characterizing the medium;  $v$  and  $c$  are the speeds of the wave in the medium and in the vacuum, respectively.

Both  $\mathbf{E}$  and  $\mathbf{B}$  are perpendicular to the direction of propagation. This feature comes from the solution of Maxwell's equations. The waves, where the direction of propagation is perpendicular to both the  $\mathbf{B}$  and  $\mathbf{E}$  vectors, are called *transverse waves*.

The physical characteristics of light depend on the electrical vector  $\mathbf{E}$ . Therefore the direction of polarization is defined by the direction of the  $\mathbf{E}$  vector. The plane wave (1) is a wave with its electric field vector always in the direction  $\mathbf{i}$ . Such a wave is said to be **linearly polarized** with polarization vector  $\mathbf{i}$  [2].

To describe a general state of polarization we need two linearly polarized waves, which are independent of each other. The waves are said to be in phase if the relative phase difference between the waves is zero or an integer multiple of  $\pm 2\pi$ . By adding the electric vectors of two linear polarized waves in phase a new linear polarized wave can be obtained. And vice versa a linear polarized wave can be divided into two perpendicular components.

One can explain this with the help of the mathematics. We have two harmonic, linearly polarized waves, which are moving through the same region of space, in the same direction, the  $z$ -direction in our case, and have the same frequency, so we can describe these electrical waves as

$$\mathbf{E}_x(\mathbf{z}, t) = \mathbf{i}E_{0x} \cos(kz - \omega t)$$

$$\mathbf{E}_y(\mathbf{z}, t) = \mathbf{j}E_{0y} \cos(kz - \omega t + \varphi)$$

where  $\mathbf{i}$  and  $\mathbf{j}$  are constant unit vectors,  $E_{0x}$  and  $E_{0y}$  are the amplitudes, which are constant in space and time, and  $k$  is magnitude of the direction of propagation vector,  $\omega$  is the angular frequency, and  $\varphi$  is the relative phase difference between the waves. The wave  $\mathbf{E}_x(\mathbf{z}, t)$  is in  $x$ - $z$  plane and  $\mathbf{E}_y(\mathbf{z}, t)$  is in the  $y$ - $z$  plane. These two waves can form a resultant linearly polarized electrical wave:

$$\mathbf{E}(\mathbf{z}, t) = \mathbf{E}_x(\mathbf{z}, t) + \mathbf{E}_y(\mathbf{z}, t) \quad (3)$$

For linearly polarized light the orientation of the electric field is constant, but its magnitude and sign vary in time. The waves are said to be in phase if  $\varphi$ , the relative phase difference between the waves, is zero or an integral multiple of  $\pm 2\pi$ . Equation (3) becomes

$$\mathbf{E}(\mathbf{z}, t) = (\mathbf{i}E_{0x} + \mathbf{j}E_{0y})\cos(kz - \omega t)$$

with fixed amplitude equal to  $(\mathbf{i}E_{0x} + \mathbf{j}E_{0y})$ , where  $\mathbf{i}$  and  $\mathbf{j}$  are constant unit vectors,  $k$  is magnitude of the direction of propagation vector,  $\omega$  is the angular frequency. This wave is also linearly polarized. (See Fig. 1.1.)

Two waves are said to be  $180^\circ$  out of phase if  $\varphi$  is an odd multiple of  $\pm\pi$ . By adding the electric vectors of two linear polarized waves out of the phase one can obtain a new linear polarized wave. This wave has  $\mathbf{E}$ -vector with another direction than resulting vector of the waves in phase. The resultant linearly polarized wave equation becomes

$$\mathbf{E}(\mathbf{z}, t) = (\mathbf{i}E_{0x} - \mathbf{j}E_{0y})\cos(k \cdot z - \omega t)$$

This wave is also linearly polarized, but the plane of vibration has been rotated as shown in figure 1.3. (and not necessarily by  $90^\circ$ )

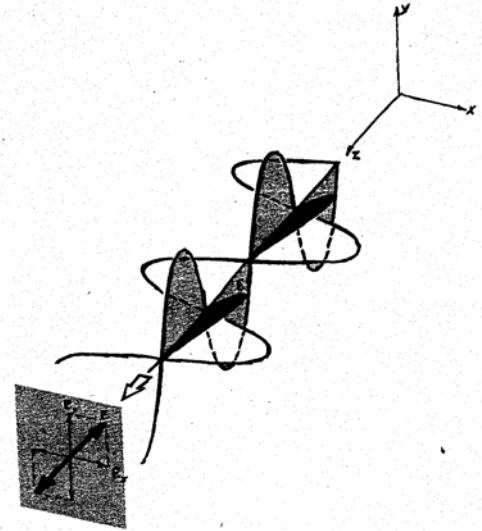


**Figure 1.1.** Linear light  $\mathbf{E}_x$  and  $\mathbf{E}_y$  are in phase because  $\varphi = 0 \pm 2\pi$ . The waves advance toward a plane of observation, where the fields are to be measured. The  $\mathbf{E}$ -field progresses through one complete oscillatory cycle as the wave advance along  $z$ -axis through one wavelength. Taken from Ref. [3].

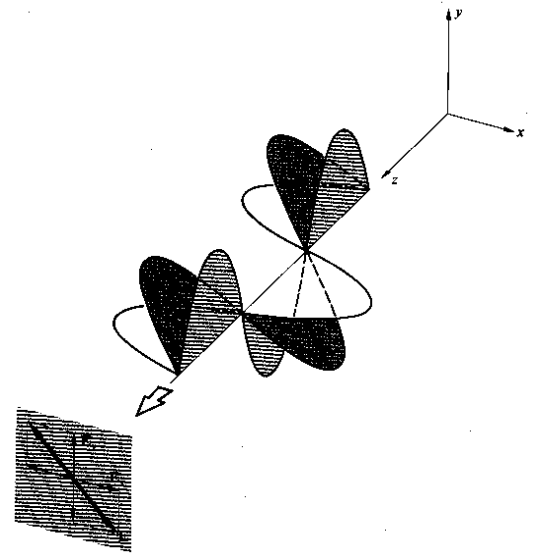


**Figure 1.2.** Linear light, where two waves are out of the phase ( $\varphi = \pm\pi$ ). The resultant wave is linearly polarized, but the plane of vibration has been rotated. Compare with **Fig. 1.1**. Taken from Ref. [3].

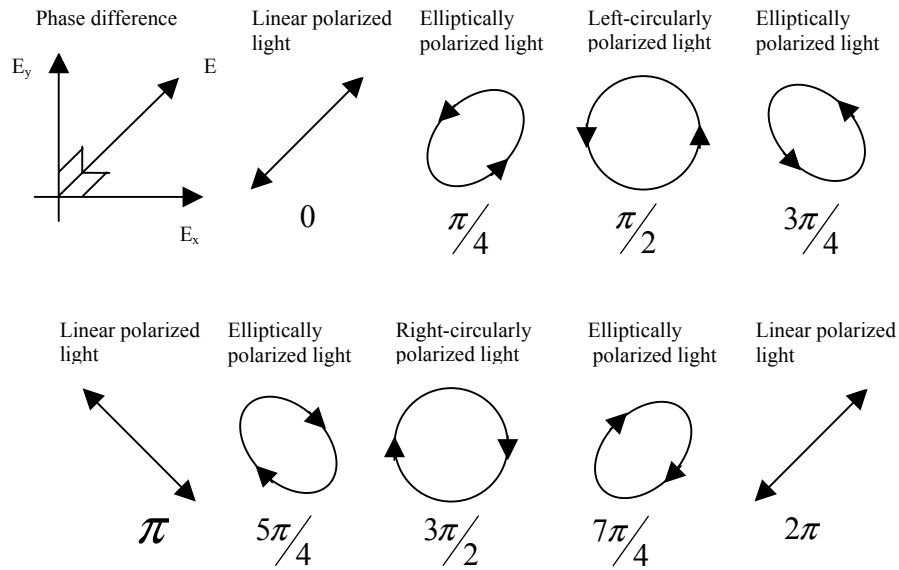


**Figure 1. 3.** The two perpendicular linearly polarized waves are added. The result, which depends on phase difference between the waves, can be another linear polarized wave, or circularly polarized wave, or elliptically polarized wave.

Linearly polarized light is a special case of elliptically polarized light. In the general case the resultant electrical field vector  $\mathbf{E}$  rotates and traces out an ellipse at the same time as the wave propagates. The circularly polarized light signifies that the  $\mathbf{E}$ -vector has constant magnitude and rotates a cycle while the wave propagates one wavelength. The circularly polarized light is also a special case of elliptically polarized light. When the relative phase difference  $\varphi$  is different from 0,  $\pi$ ,  $2\pi$  etc the result became **elliptically polarized light**. Only when the phase difference is  $\frac{\pi}{2}$ ,  $\frac{3\pi}{2}$ ,  $\frac{5\pi}{2}$  etc. the result is called the **circularly polarized light** (See Fig. 1.3.).

The linearly polarized light can be obtained by transition of natural light through the polarizer. If natural light passes through no ideal polarizer it became partly polarized i.e. the amplitude of the electrical field vector in one direction is higher than the amplitudes of the electrical field vectors in other directions. By transmitting this partly polarized light through another polarizer the intensity of the light can vary from  $I_{\max}$  to  $I_{\min}$  by rotating the device with angle  $\pi/2$ . The following expression is defined as the polarization of light

$$P = \frac{I_{\max} - I_{\min}}{I_{\max} + I_{\min}}$$

For linearly polarized light  $I_{\min} = 0$  and  $P = 1$ . For unpolarized light  $I_{\max} = I_{\min}$  and  $P = 0$ .

### 1.3 Polarization of $\gamma$ -rays.

$\gamma$ -rays are also electromagnetic waves with wavelengths between  $10^4$  and 100 fm, which interact with matter through three processes, namely photoelectric absorption, Compton scattering and pair production. Compton scattering is the process involved in measurement of the polarization of the  $\gamma$ -rays. In Compton scattering a photon scatters from a nearly free atomic electron, resulting in a less energetic photon and a scattered electron carrying the energy lost by the photon [4]. The polarization of  $\gamma$ -rays is sensitive to Compton scattering in the sense that the direction of the scattered photon is perpendicular to the direction of the electric vector of the incident photon. This dependence can be seen from the Klein-Nishina cross-section formula for linearly polarized photons. The formula, taken from Ref. [5], is

$$\frac{d\sigma^{KN}}{d\Omega}(\theta, \phi) = \frac{r_0^2}{2} \left( \frac{E'}{E} \right)^2 \left( \frac{E'}{E} + \frac{E}{E'} - 2 \sin^2 \theta \cos^2 \phi \right)$$

where  $r_0$  is the classical electron radius,  $r_0 = \frac{e^2}{4\pi\epsilon_0 mc^2} = 2.818 \text{ fm}$ ,  $E$  and  $E'$  are the energies of the incoming and outgoing photon, respectively,  $\theta$  is the angle of the outgoing photon with respect to the incident photon, and  $\phi$  is the angle between the electric vector of the incident  $\gamma$ -ray and the plane containing the incident and scattered  $\gamma$ -ray (see Fig. 1.4.).

This formula gives that the cross section for scattering is maximum when  $\phi = 90^\circ$ , i.e. the scattered photon prefers the direction perpendicular to the incident polarization (perpendicular to the direction of the E-vector of the incident photon). The  $\gamma$  intensity  $I$  at an angle  $\theta$  relative to the beam axis varies with the electric or magnetic nature of the transition and its multipolarity. The degree of linear polarization depends on the angle  $\phi$  between the electric vector  $E$  of the radiation and the reaction plane containing the angle  $\theta$ .

Linear polarization of  $\gamma$ -rays,  $P(\theta)$ , is defined as the difference between the intensities of the radiations presenting an electric vector parallel to the reaction plane ( $\phi = 0^\circ$ ) and the electric vector perpendicular to that plane ( $\phi = 90^\circ$ ).  $P(\theta)$  is normalized to the total intensity and written as [6]:

$$P(\theta) = \frac{I(\theta, \phi = 0^\circ) - I(\theta, \phi = 90^\circ)}{I(\theta, \phi = 0^\circ) + I(\theta, \phi = 90^\circ)}$$

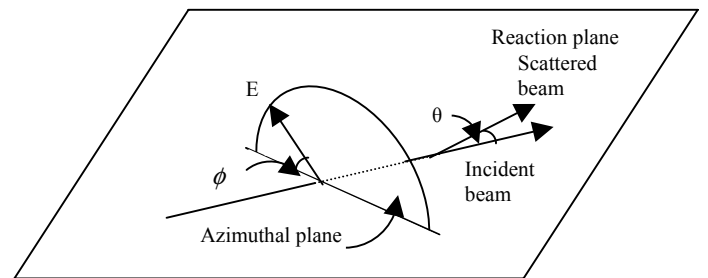


**Figure 1.4.** Angles and vectors involved in a reaction sensitive to the linear polarization of a  $\gamma$ -ray.

where  $\theta$  is the polar Compton scattering angle (the angle between incident and scattered  $\gamma$ -rays) and  $\phi$  is the azimuthal scattering angle (the angle between the electric vector of the incident  $\gamma$ -ray and the plane containing the incident and scattered  $\gamma$ -ray).  $I(\theta, \phi = 0^\circ)$  is the average component intensity of the  $\gamma$ -ray electric vector in the reaction plane (the plane containing the incident particle beam and the outgoing  $\gamma$ -ray),  $I(\theta, \phi = 90^\circ)$  is the intensity perpendicular to this plane.

The linear polarization  $P(\theta)$  is proportional to experimental asymmetry. The experimental asymmetry  $A$  can be determined by formula

$$A = \frac{a(E_\gamma)N_v(\theta) - N_h(\theta)}{N_v(\theta) + N_h(\theta)},$$

where  $a(E_\gamma)$  is normalization constant,  $N_v(\theta)$  and  $N_h(\theta)$  are numbers of up-down and left-right counts, respectively. (See more about the asymmetry  $A$  in the analysis sections). At low energies such asymmetry should be maximum for  $\theta = 90^\circ$  [5]. The asymmetry  $A$  and the polarization  $P$  are linked by the relation  $A = QP$ , where  $Q$  is so called polarization sensitivity of the experimental set-up (distance to the target and internal geometry of the detector).  $Q$  is a function of the incident  $\gamma$ -ray energy. The procedure of the measurement of  $Q$  is the following. Using  $\gamma$ -rays of known polarization, asymmetries can be measured and then  $Q$  can be determined using  $A = QP$ . The polarization sensitivity dependence on the  $\gamma$  energy is schematically shown in Fig. 1.5.

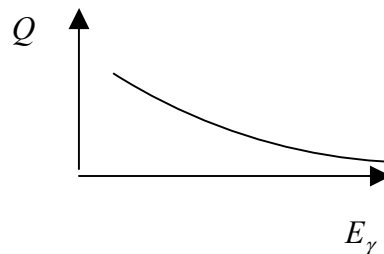


**Figure 1.5.** shows how the polarization sensitivity  $Q$  is depended on the  $\gamma$ -ray energy.

## 2. Experimental methods

### 2.1. The experiment

The experiment was carried out in 6 days in fall 1998 at a laboratory in Italy. The experiment used the reaction  $^{40}\text{Ca}(^{24}\text{Mg},\text{xpynz}\alpha)$  at 96 MeV beam energy. The enriched  $0.5\text{-mg/cm}^2$  thin  $^{40}\text{Ca}$  layer was backed by  $7.0\text{-mg/cm}^2$  gold and covered by an additional thin gold layer to prevent its oxidation.

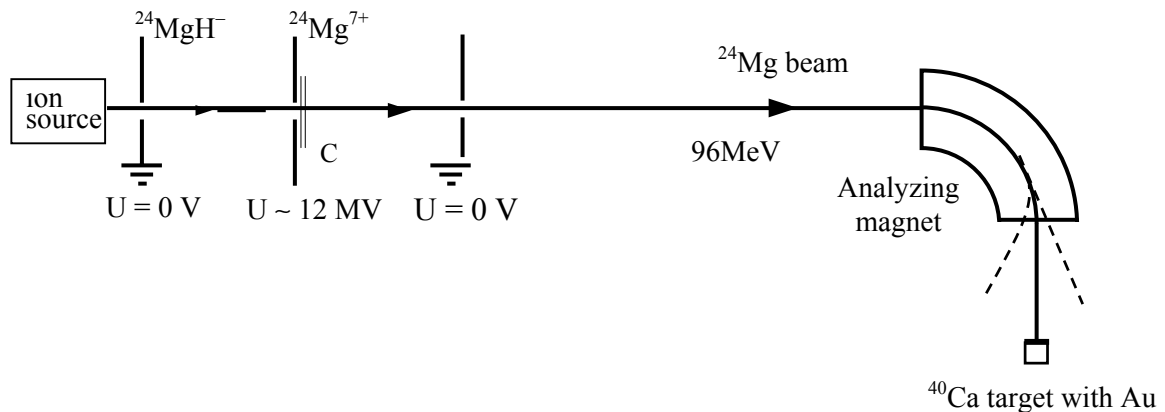


**Figure 2.1.** The  $^{24}\text{Mg}$  beam hits the  $^{40}\text{Ca}$  target at 96 MeV after having been accelerated twice over a potential fall of 12 MV. Based on a picture in [7].

The negative  $\text{MgH}^-$  ions were accelerated in an electric field of the Tandem Van de Graaff XTU accelerator at Laboratori Nazionali di Legnaro toward the high voltage terminal (see Fig. 2.1.). There they passed through a thin foil of carbon, loose a certain number of electrons, and became positive ions  $^{24}\text{Mg}^{7+}$  and then directed towards the  $^{40}\text{Ca}$  target placed inside the detection system.

## 2.2. Fusion-evaporation reaction

The aim of my master thesis project is to measure the linear polarization of  $\gamma$ -rays in a number of nuclei in the mass  $A \approx 60$  region namely  $^{56,57}\text{Co}$ ,  $^{58-60}\text{Ni}$ ,  $^{60,61}\text{Cu}$  and  $^{61}\text{Zn}$ . These nuclei are produced when an accelerated projectile nucleus  $^{24}\text{Mg}$  collides and fuses with a target nucleus  $^{40}\text{Ca}$ . The process is schematically illustrated in figure 2.2.

The beam nucleus  $^{24}\text{Mg}$  accelerates and collides with the target nucleus  $^{40}\text{Ca}$ . The compound nucleus  $^{64}\text{Ge}$  is very excited and cools down by evaporation of neutrons, protons, and alpha particles according to  $^{24}\text{Mg} + ^{40}\text{Ca} \rightarrow ^{64}\text{Ge}^* \rightarrow xp + yn + z\alpha + ^A\text{X}$ .

This de-excitation process can occur in many different ways depending on the combination of the evaporated protons, neutrons, and alpha particles. After the evaporation process, when the particle emission is no longer energetically possible, the residual nucleus loses its energy by the emission of  $\gamma$ -rays.

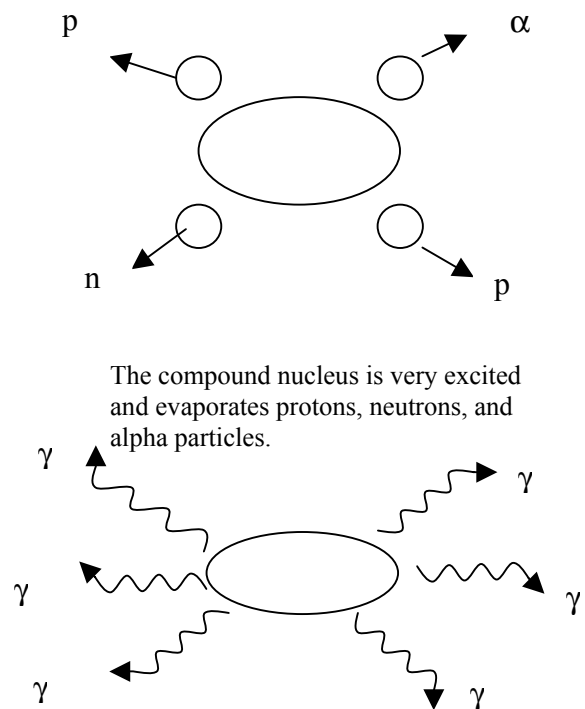
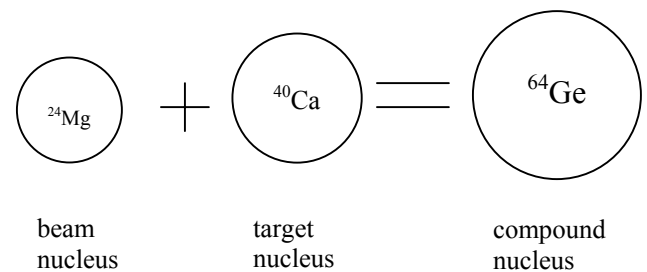
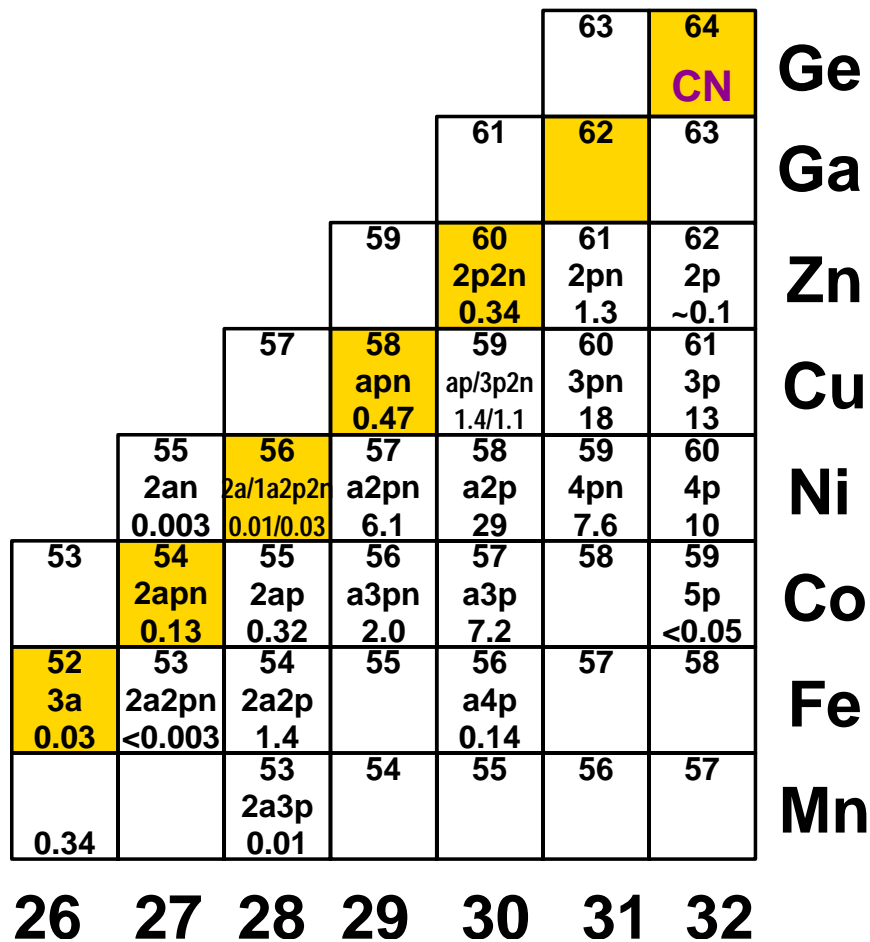


**Figure 2.2.** Scheme of the fusion-evaporation reaction.



Populated nucleus            →     ${}^A X$   
 Reaction channel            →     $\alpha pn$   
 Relative cross section (%)    →    10

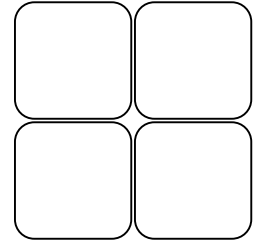
**Figure 2.3.** Experimental relative cross section of the nuclei identified in the experiment. The number number of neutrons are given on the x-axis. The  $N=Z$  nuclei having the same number of neutrons and the number of protons are indicated by the gray squares. The symbols of the nuclei are indicated on the right hand side. Top right is the compound nucleus  ${}^{64}\text{Ge}^*(\text{CN})$ .

Fig. 2.3. shows the different reaction channels, which were open in the experiment. Top right is the compound nucleus  ${}^{64}\text{Ge}^*$ . Every channel corresponds to a nucleus. For instance,  ${}^{57}\text{Ni}$  is produced by emission of one  $\alpha$ -particle, two protons, and one neutron (the  $\alpha 2pn$  channel),  ${}^{60}\text{Ni}$  is produced through the  $4p$  channel. The nucleus  ${}^{56}\text{Ni}$  can be produced through two different reaction channels namely by  $2\alpha$  emission or as the  $\alpha 2p2n$  channel. In the figure one can see the populated nucleus, the corresponding reaction channel, and its relative cross section in percent. The latter indicates the probability for a nucleus to be formed during the reaction process. Some channels are strong and some channels are weak. The strongest channel is  ${}^{58}\text{Ni}$  with a cross section  $\sigma_{rel} = 29\%$ . Other strong

channels are  $^{60}\text{Cu}$  (18%),  $^{61}\text{Cu}$  (13%), or  $^{60}\text{Ni}$  (10%). The nucleus  $^{59}\text{Cu}$ , which can also be produced through two different reaction channels,  $\alpha p$  or  $3p2n$ , has also two different cross sections 1.4% and 1.1%, respectively.

### 2.3. Detectors

$\gamma$ -rays were measured with high-purity germanium detectors (HPGe) in the experiment. Such detectors have relatively high efficiency in detecting incident  $\gamma$ -rays, very good energy resolution resulting in very narrow peaks in the spectra, and a reasonable ratio of full-energy to partial-energy events. A large number of detectors in modern spectrometers (~100-200) provide high granularity to localize individual  $\gamma$ -rays and reduce the probability of two  $\gamma$ -rays hitting one detector in the same event [8]. The functioning of Germanium detectors, like almost all detectors, is based on an electric field to separate electrons or holes from atoms and count these separated charge carriers. Electrons and holes are formed as result of the interaction of  $\gamma$ -rays with the detector material. The amplitude of the output signal is proportional to the number of electrons and holes formed by the radiation, i.e., depends on the energy of  $\gamma$ -rays.



**Figure 2.4.** Schematic view of a clover detector (front).

A typical Germanium detector has a cylindrical shape with diameter and length of about 7-9 cm (see Fig. 2.5) An incident 1 MeV  $\gamma$ -ray produces a full energy peak with a resolution of about 2 keV. In the experiment the polarization was measured with clover detectors. The detectors consist of four Germanium crystals. The principle behind clover detectors is to use the polarization dependence on Compton scattering. The four Germanium crystals lie in a plane perpendicular to the  $\gamma$  beam direction.

Each crystal works as an analyzer and also as a scatterer.

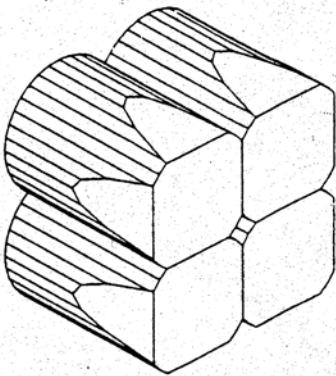


**Figure 2.5.** Clover detector. Taken from Ref. [9].

A Germanium detector is a semiconductor detector and for  $\gamma$ -ray detection preferred to Silicon detectors because of its higher atomic number. As the photoelectric cross section is proportional to  $Z^5$ , this leads to a higher probability to detect full energy peaks. It is also easier to excite the electrons from the valence band into the conduction band in Germanium than in Silicon. Germanium atoms form a solid crystal and have four valence electrons in the valence band. These four valence electrons form covalent bonds with other electrons from neighbouring atoms (see Fig. 2.6). The valence band is filled and conduction band is empty. The energy gap is about 1 eV, and at room temperature some of the electrons are thermally excited across the gap into the conduction band (see Fig. 2.7).

Some of the neighbouring electrons move to the hole and leave a new hole behind. The hole appears to migrate through the crystal. The electrons in the valence band are bound and cannot move freely. The conductivity rises with temperature. Therefore Germanium detectors must be operated at low temperatures to avoid the thermal excitation. One can also control electrical conduction in semiconductors and add small amounts of material called dopants. There are two types of dopants, p-type and n-type. In the n-doping process valence-5 impurity atoms are added. These impurity atoms (P, As, Sb) change place with a Germanium atom. Four valence electrons from the impurity atom are bonded, the fifth electron moves freely in the conduction band. In the p-doping process the valence-3 impurity atoms are added instead. The impurity atom can bound an electron from another Germanium atom. A hole, which can move in valence band, is created. One wants to avoid the current through the semiconductor when we place it between two electrodes and apply a voltage. Therefore, we can bring in contact p- and n-type materials. The electrons from the n-type material can diffuse across the junction to the p-type material, and combine with the holes. In the vicinity of the junction the charge carriers are neutralized and there space charges on the both sides of the junction, positive on the n-side and negative on the p-side, which create an field. This electrical field resists the diffusion of electrons and holes, creating a region called **depletion region**.

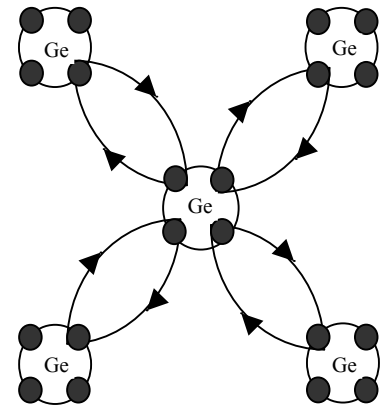


**Figure 2.6.** Germanium atom has four valence electrons in the valence band.

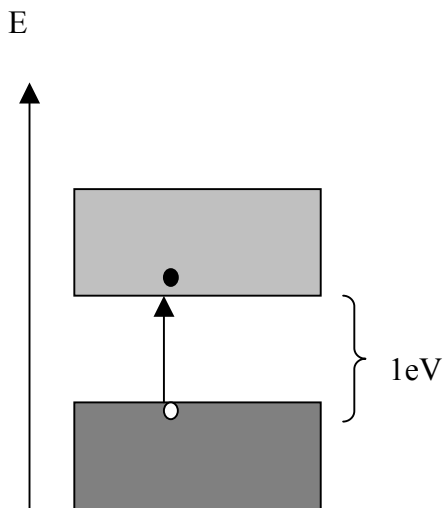


**Figure 2.7.** There are two highest bands in Germanium crystal, valence band and conduction band. The energy gap between these bands is about 1eV. Migrations of electrons through the forbidden zone create prerequisites for electrical conduction in the crystal.

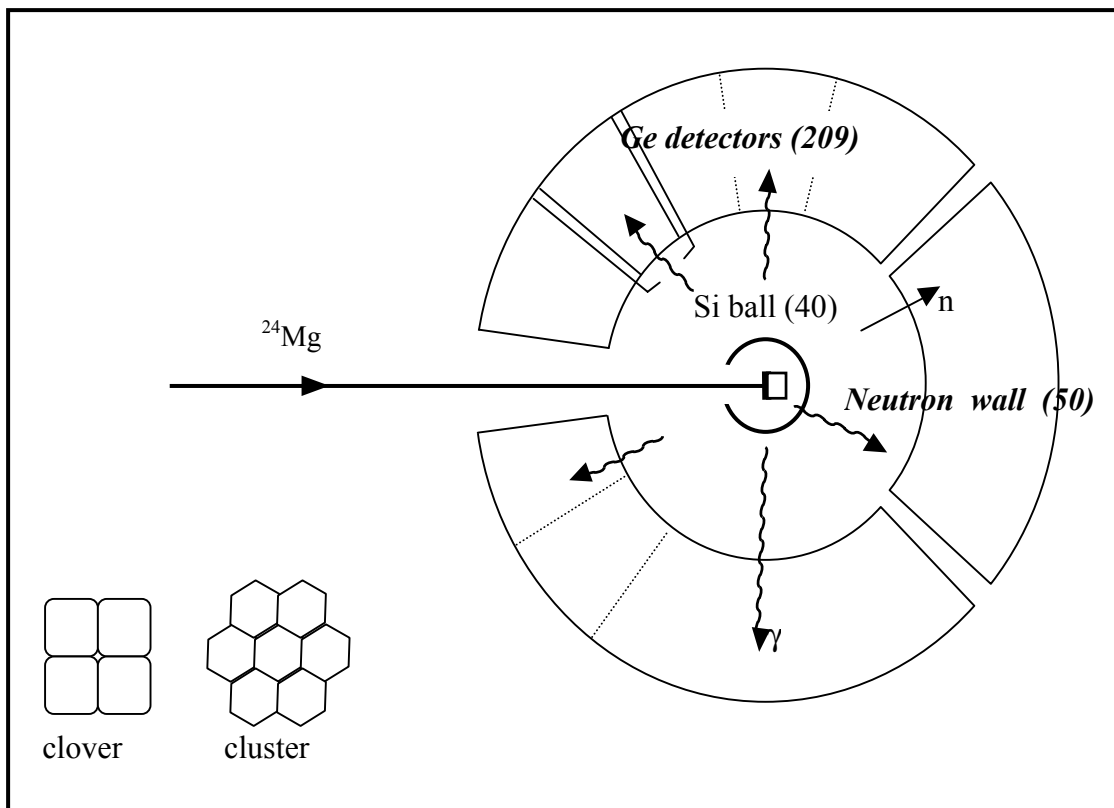
One wants to avoid the current through the semiconductor when we place it between two electrodes and apply a voltage. Therefore, we can bring in contact p- and n-type materials. The electrons from the n-type material can diffuse across the junction to the p-type material, and combine with the holes. In the vicinity of the junction the charge carriers are neutralized and there space charges on the both sides of the junction, positive on the n-side and negative on the p-side, which create an field. This electrical field resists the diffusion of electrons and holes, creating a region called **depletion region**.

High Purity Germanium detectors were used in the experiment. For this detector to be suitable as a photon detector it must be free from impurity atoms causing doping. The concentration of the impurity atoms in this kind of detectors must be so low that the conductivity is not affected and we have a region where we can have a strong electric field without any electrical current. However, there must still be a P-N junction. Therefore, a thin layer of lithium atoms is diffused on one side of the crystal. When  $\gamma$ -rays enter the detector they interact with electrons in the crystal.

$\gamma$ -rays interact with matter through three processes, namely photoelectric absorption, Compton scattering, and pair production. In photoelectric process the energy of  $\gamma$ -rays is relatively small such that incident photons are completely absorbed in one interaction. In the Compton scattering process the incoming photon transfers only a part of its energy to an electron in the Germanium detector. The outgoing photon can escape from the detector resulting a large, continuous background, and interact once more in the crystal. To reduce unwanted Compton scattered events in the data, there are bismuth germanate scintillator crystals, BGO crystals, which surround every Ge-detector.

## 2.4. EUROBALL detection system

The data I have analyzed comes from an experiment carried out at the Laboratori Nazionali di Legnaro in Italy using the EUROBALL Ge-detector array [9], the neutron wall for detection of evaporated neutrons, and Si ball for detection of charged particles. In this configuration EUROBALL itself consists of 209 Germanium crystals, which are grouped in 15 cluster detectors and 26 clover detectors. A cluster detector contains seven individually encapsulated germanium crystals. Each clover detector consists of four separate germanium crystals packed together in the four-leaf clover arrangement.



### 3. Data analysis

#### 3.1. Identification of $\gamma$ -rays.

In fusion-evaporation reactions aiming at proton-rich nuclei many reaction channels are opened (see Fig. 2.3.). About 30 excited nuclei were populated in the present experiment, and all these nuclei have different production cross-sections. In my master thesis project I treated the full data set, i.e., no coincidences with evaporated particles were required. Only in specific cases spectra in coincidence with one or more neutrons were investigated. Fig. 3.1. shows the so called total projection of one of the  $\gamma - \gamma$  matrices, which were analysed.

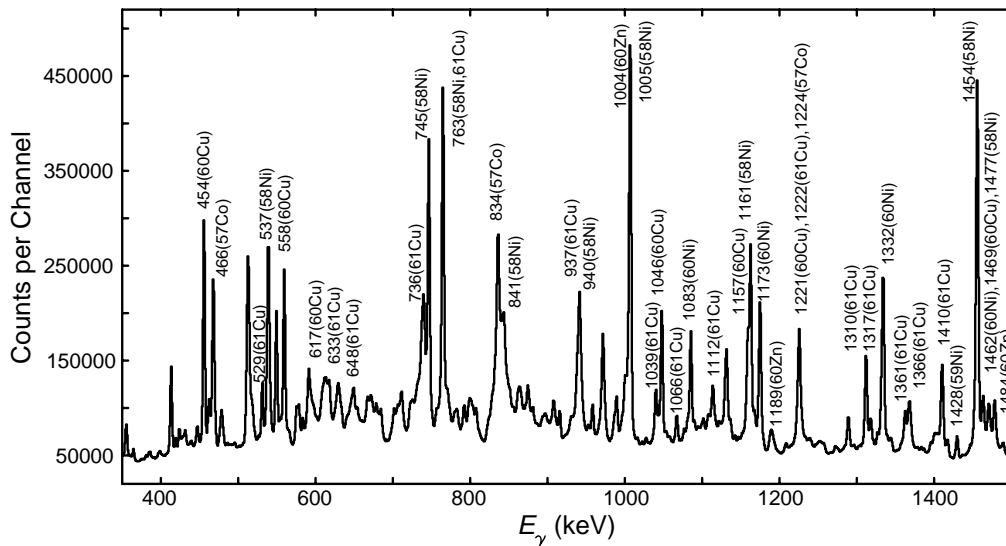


**Figure 3.1.** A part of the total projection onto one axis of one of the  $\gamma - \gamma$  matrices used in the analyse is shown. Peaks are labeled with their energies in keV and the respective residual nuclei, which were produced in the fusion-evaporation reaction.

There are basically transitions from all residual nuclei produced in the reaction. The highest peaks belong to the nuclei, which have a large cross section in the fusion-evaporation reaction. For instance,  $^{58}\text{Ni}$  and  $^{60}\text{Cu}$  are the two nuclei, which have the two largest relative cross sections, 29% and 18% respectively. Figure 3.1 shows intense 537-, 745-, 763-, 1005-, 1161-, 1454-keV transitions belonging to  $^{58}\text{Ni}$ , and the 454-, 558-, 1046-, and 1157-keV transitions belonging to  $^{60}\text{Cu}$ . The less cross section a nucleus has the smaller are its peaks. For instance,  $^{59}\text{Ni}$  has a relative cross section of 7.6% represented by the peak at 1428 keV. Some peaks comprise the statistics from several nuclei at the same time. For example, the peak at 1005 keV has statistics from  $^{58}\text{Ni}$  and  $^{60}\text{Zn}$ .  $^{58}\text{Ni}$  and  $^{60}\text{Zn}$  have relative cross sections of 29% and

0.34%, respectively, and therefore is the amount of the  $^{60}\text{Zn}$  tremendously small in this transition. The 763-keV peak has a large amount of  $^{58}\text{Ni}$  and a smaller amount of  $^{61}\text{Cu}$ . The identification of  $\gamma$ -rays from different nuclei in the total projection was the first step in my work. It was necessary for the further analysis to identify the “cleanest” peaks in the total projection, i.e., peaks, which contain statistics from possibly only one nucleus.

### 3.2. $\gamma$ - $\gamma$ coincidence matrix

Two  $\gamma$ -rays are said to be in coincidence with each other if they are detected simultaneously, which means that the time interval between them is not more than  $\sim 10^{-8}$  s. Such events can be placed in a  $\gamma$ - $\gamma$  coincidence matrix. For example  $\gamma$ -rays with energies of 970-, 1444-, and 1366 keV are detected simultaneously. The energy transition of 970 keV is in coincidence with 1444- and 1366 keV transitions. They follow each other in a sequence (see the energy level diagram, Fig. 4.2.) and are not parallel. By doing a  $\gamma$ - $\gamma$  coincidence matrix one can organize these transitions in the following way:

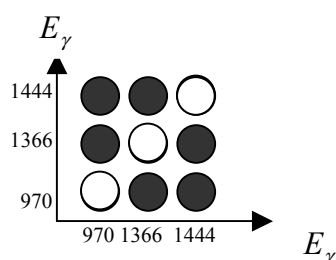


**Figure 3.2.**  $\gamma$ - $\gamma$  coincidence matrix for the 970-, 1366-, and 1444 keV transitions.

In the column of the 970 keV transition the two filled circles are placed in the rows of the 1366- and 1444 keV transitions, and in the row of the 970 keV transition two filled circles are placed in the columns of the 1366- and 1444 keV. The 970 keV transition cannot be in coincidence with itself. Therefore the matrix element [970,970] is shown with an open circle. In the same way one can handle the 1366- and 1444 keV transitions.

There are several other lines in coincidence with the 970 keV line, namely at 972-, 670-, 648-, 1330-, or 1042 keV. But the 972- and 670 keV transitions are not in coincidence with each other. The 1330 keV line is in coincidence with 648-, 670-, 972-, 970-, 529-, 736-, 1532-, and 1527 keV, but not with 1042-, 936-, 1366-, and 1444 keV. Figure 3.3(a) shows an example of a bigger  $\gamma$ - $\gamma$  coincidence matrix, which contains all these transitions described above. Filled circles indicate matrix elements of two transitions, which are in coincidence with each other; the open circles mark the matrix elements with transitions not in coincidence. A  $\gamma$ - $\gamma$  coincidence matrix helps us to organize all these transitions to get a better view, which transitions

are in coincidence and which are not. This knowledge about transition coincidence can be used to determine the energy level diagram of the nucleus.

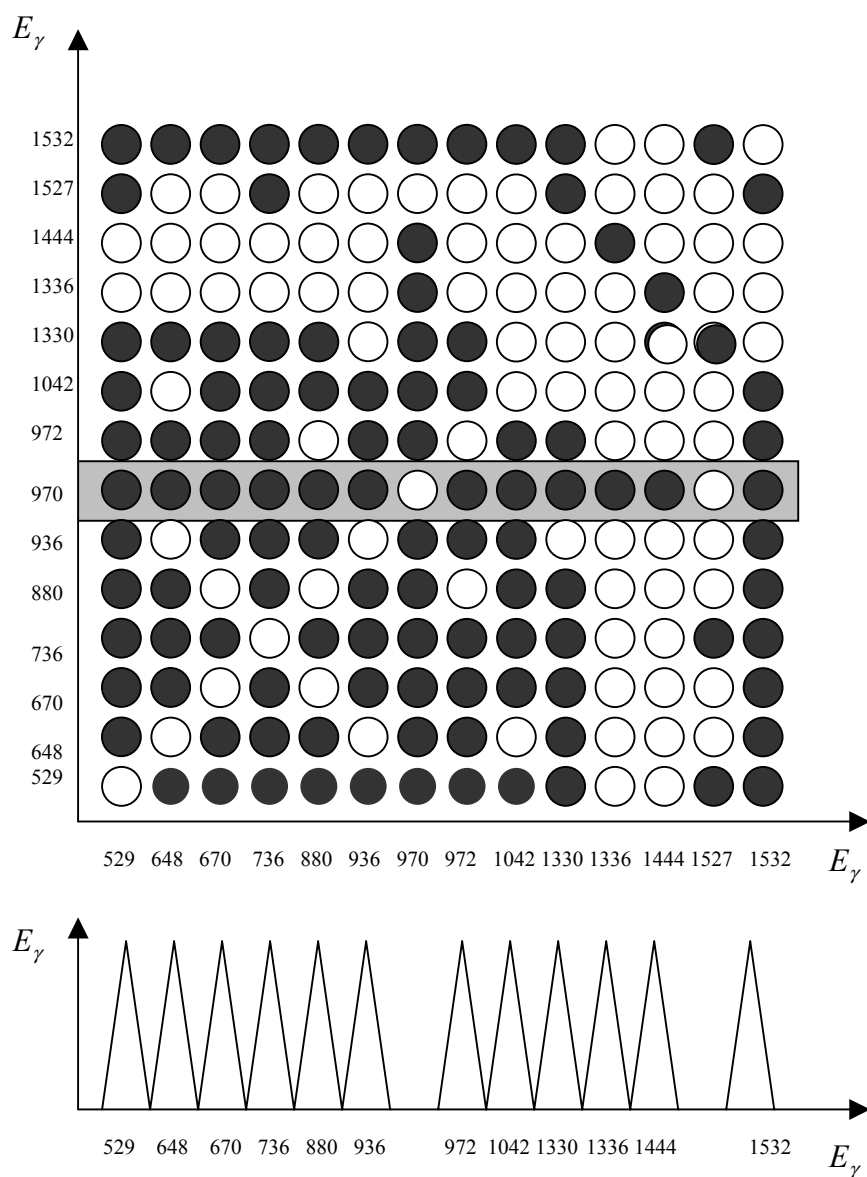


**Figure 3.3.** Panel (a) shows the  $\gamma$ - $\gamma$  coincidence matrix for the 529-, 648-, 670-, 736-, 880-, 936-, 970-, 972-, 1042-, 1330-, 1336-, 1444-, 1527-, and 1532 keV transitions. Panel (b) shows the projection of the events coincident with the 970 keV line.

Projecting the events coincident with one of the  $\gamma$ -rays in this matrix (here 970 keV) on one axis one obtains the  $\gamma$ -ray spectrum sketched on the bottom of Fig. 3.3(b). The reader can compare this projection with the real spectrum shown in Fig. 3.4(a). Because of weak connection between the 970- and 1532 keV transitions it is difficult to see a peak at 1532 keV in the real spectrum.

### 3.3. Collection of statistics.

To be able to measure  $\gamma$ -ray polarization in one specific nucleus it is better to examine spectra, which comprise only transitions from this nucleus, and not the total projection.

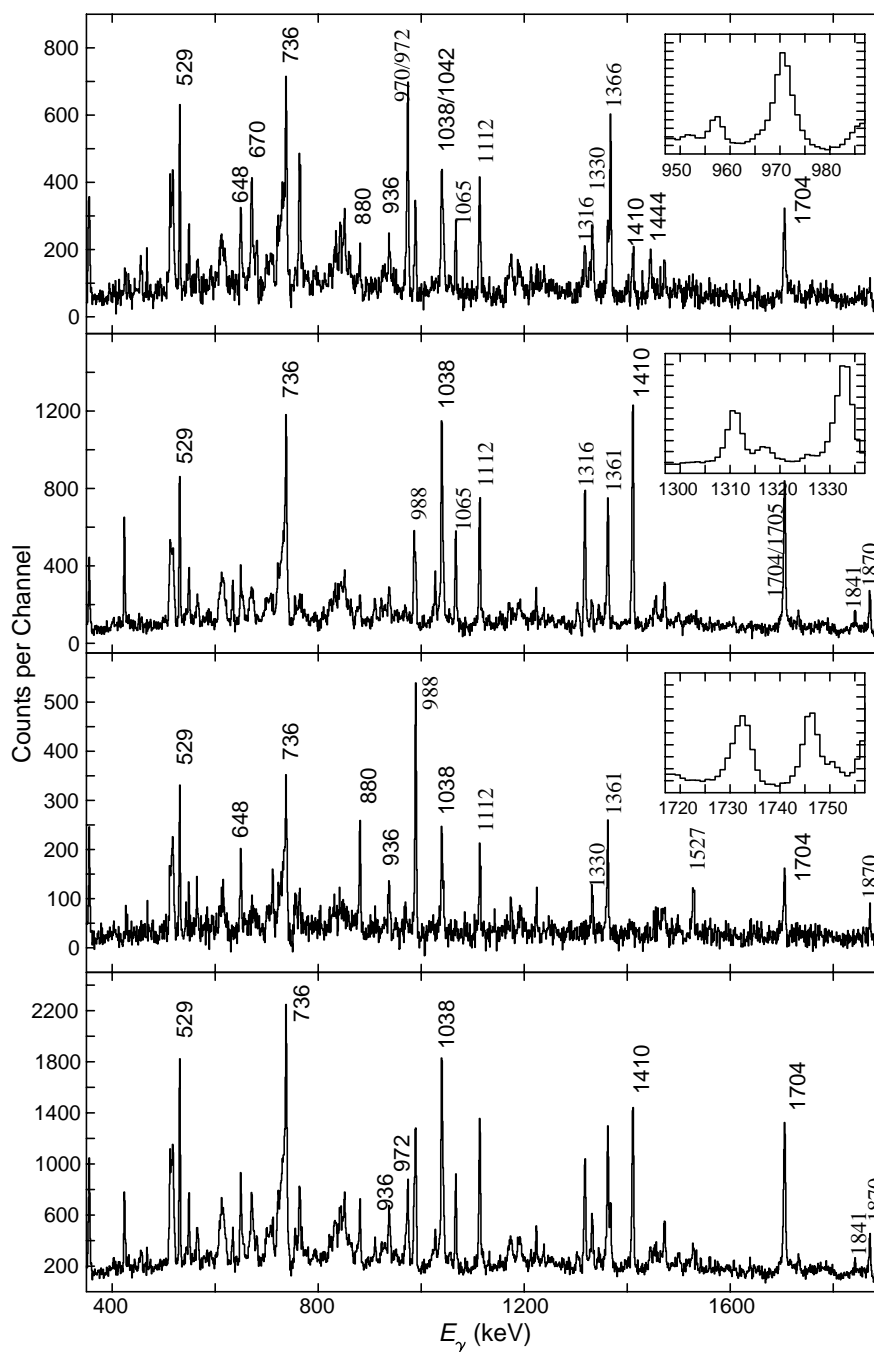


**Figure 3.4.** Panels (a), (b), (c) show  $\gamma$ -ray spectra in coincidence with the 970-, 1310-, and 1733-keV lines in  $^{61}\text{Cu}$ , respectively. Panel (d) shows the sum of the 970-, 1310-, and 1733-keV gated spectra.

For the spectra to be as clean as possible a cut on the “cleanest” peaks is made in the total matrix. For this case the  $\gamma-\gamma$  coincidence matrix is used, i.e., by doing a cut on the cleanest peaks it is possible to see which of the other peaks are in coincidence with the first one. As an example I am using  $^{61}\text{Cu}$ . 970-keV is one of the cleanest peaks in the total projection. By doing a cut on the peak with energy 970 keV we should be able to see, for example, peaks at 1366-keV and 1444-keV. This coincidence relationship among the 1444-, 1366-, and 970-keV transitions suggests that they follow one another in a cascade. Figure 3.4(a) shows that there are several other transitions in coincidence with the 970-keV line namely the sequence of 972-, 670-, 936-, 1042-, 529-, 736-, and 1532-keV transitions. The excited nucleus can decay by the 529-1330-1527-648 keV cascade or by the 648-670-972-970 keV cascade starting from the 3260 keV state. All these transitions are seen in Fig. 3.4(a).

However, the peaks with 1310- and 1733-keV are not seen, because they are parallel to the 970 keV transition. It is simply not possible for the nucleus to first be deexcited by the transition 970- and then 1310- and 1733-keV, nor can it decay from a level of 1310-keV with a transition of 1310-keV and then 970-keV. The transitions 970-, 1310- and 1733-keV are not in coincidence with each other. A look at the spectra gated by the 1310-keV transition shows that the 1316-, 1841-, 1410-, 1361-, 1038-, 1361-, 1038-, 1704-, 1112-, 1472-, 736-, 1705-, 1065-, 1870-, 529-keV transitions are in coincidence with 1310 keV line. The nucleus can deexcite by several sequences, for example, 1472-, 1112-, 1704-, 1038-, 1361-, 1410-keV or 736-, 529-, 1870-, 1410-, 1310-keV, or 736-, 1038-, 1065-, 1705-keV etc. All these transitions are present in Fig. 3.4(b). Similarly, the 1733 cut spectrum, Fig. 3.4(c), shows that the 1704-, 1527-, 1330-, 529-, 988-, 880-, 648-, 936-keV transitions are in coincidence with the 1733 keV line, but not with 1310- and 970-keV. Fig. 3.4(d) represents the sum of all the three previous spectra (see the scale of the y-axis). The sum –spectrum shows the peaks from the three spectra. This may give us more statistics of the peaks existing in more than one spectrum, which helps us getting more accurate asymmetry values.

### 3.4. Measurement of $\gamma$ -ray intensity.

As described in the theory section the polarization of  $\gamma$ -rays is defined as the difference between the intensities of the radiation presenting an electric vector parallel to the reaction plane and the electric vector perpendicular to that plane. The polarization and the asymmetry are related to each other by the formula  $A = QP$ , where  $Q$  is the polarization sensitivity of the detector (see the theory section). Therefore, to determine polarization it is enough to determine the asymmetry. To determine the asymmetry the clover detectors collecting the statistics from up-down and left-right scattered events in the experiment have to be considered.

Fig. 3.5. shows a situation whereby a  $\gamma$ -photon with vertical electric vector is incident on the detector. According to the Klein-Nishina cross section formula (see the theory section) the left-

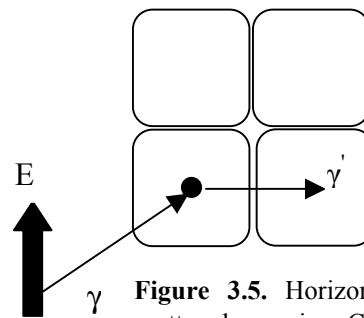


**Figure 3.5.** Horizontally scattered  $\gamma$ -ray in a Clover detector.

right scattering is most probable here. By measuring the number of up-down (out of reaction plane) counts and left-right (in reaction plane) counts the experimental asymmetry  $A$  can be determined (See the theory section).

The statistics from the “up-down” and the “left-right” scattered events were placed in the “vertical” and “horizontal”  $\gamma-\gamma$  coincidence matrices, respectively. Both matrices contained the statistics from all the nuclei in the fusion-evaporation reaction. By gating on the “cleanest” and the “strongest” peaks in the both matrices I got two spectra, “horizontal” and “vertical”, for every gated transition. After the collection of statistics, i.e., summing several cuts, “horizontal” and “vertical” spectra for every nucleus were obtained. Then I measured the intensity of every relatively strong transition by determining the area of the corresponding peak in both the “horizontal” and “vertical” spectra. These numbers including uncertainties were rewritten as an input file for a computer program. For stretched transitions the asymmetry values are negative if the transition had a magnetic character and positive if the transition was electric. Fig. 3.6. shows  $^{61}\text{Cu}$  sum-spectra gated on 1038- and 1361 keV transitions from the “horizontal” and the “vertical” matrix in the same picture. The gray color represents the spectrum from the “horizontal” matrix while the black color represents the spectrum from the “vertical” matrix.  $^{61}\text{Cu}$  has a transition 1038 keV, which is already known as E2. The black peak is higher than the gray peak for this transition. This transition can be used as reference. Fig. 3.6. shows that for the transitions at 1065-, 1038-, 988-keV the black peaks are higher than the gray peaks. The corresponding asymmetry values are positive and these  $\gamma$ -transitions have electric character. The 736-keV line is an M1-transition: the gray peak is higher than the black one and the asymmetry value is negative. The 970-keV transition is a mixture of M1 and E2. One can see that the heights of the peaks are almost the same in the figure (the asymmetry value is +0.012(21), see table for  $^{61}\text{Cu}$  in the result section).

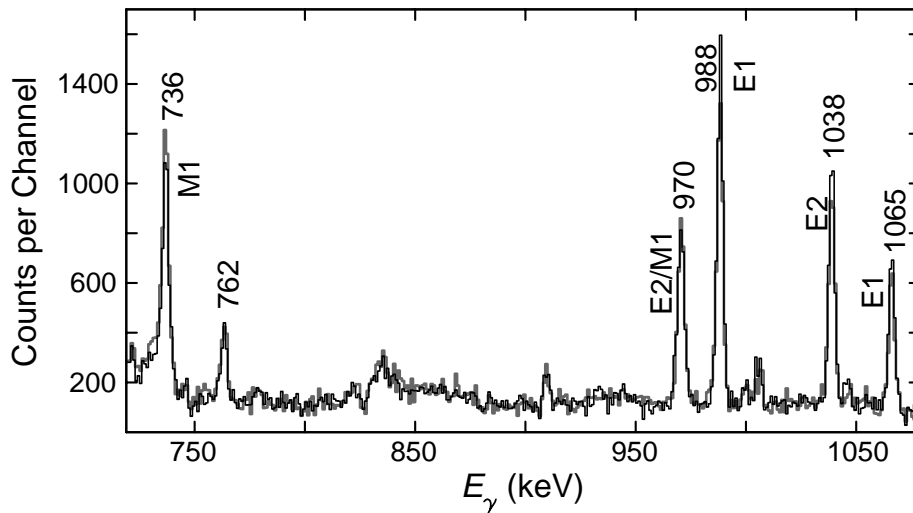


**Figure 3.6.** Spectra from the “horizontal”(gray) and the “vertical”(black) matrix for  $^{61}\text{Cu}$ .

### 3.5. Normalization of the spectra and DCO-ratios.

The detection efficiencies of all possible “horizontal” and “vertical” combinations of the 26 clover detectors used in the experiment are not necessarily identical. Therefore, a calibration has to be performed to ensure that the number of “horizontal” counts,  $N_h$ , equals the number of “vertical” counts for unpolarised  $\gamma$  radiation of energy  $E_\gamma$ . This normalization can be done by looking at isotropic radiation from a calibration source like, in this case,  $^{152}\text{Eu}$ . Normalization coefficients  $a(E_\gamma) = \frac{N_h}{N_v}$  can be determined for a numbers of transitions from  $^{152}\text{Eu}$   $\gamma$ -decay. They are plotted in Fig. 3.7. as filled squares. The uncertainties,  $\Delta a(E_\gamma)$ , have been derived from standard error analysis, i.e.,

$$\Delta a(E_\gamma) = a(E_\gamma) \sqrt{\left(\frac{\Delta N_h}{N_h}\right)^2 + \left(\frac{\Delta N_v}{N_v}\right)^2}, \text{ using } \Delta N_i = \sqrt{N_i}, i = h, v$$

Subsequently, a linear regression including the uncertainties of the individual data points was performed yielding the coefficients  $m=1.62519 \cdot 10^{-5} \text{ (keV)}^{-1}$  and  $n=0.9854$  for the relation  $a(E_\gamma) = mE_\gamma + n$ .

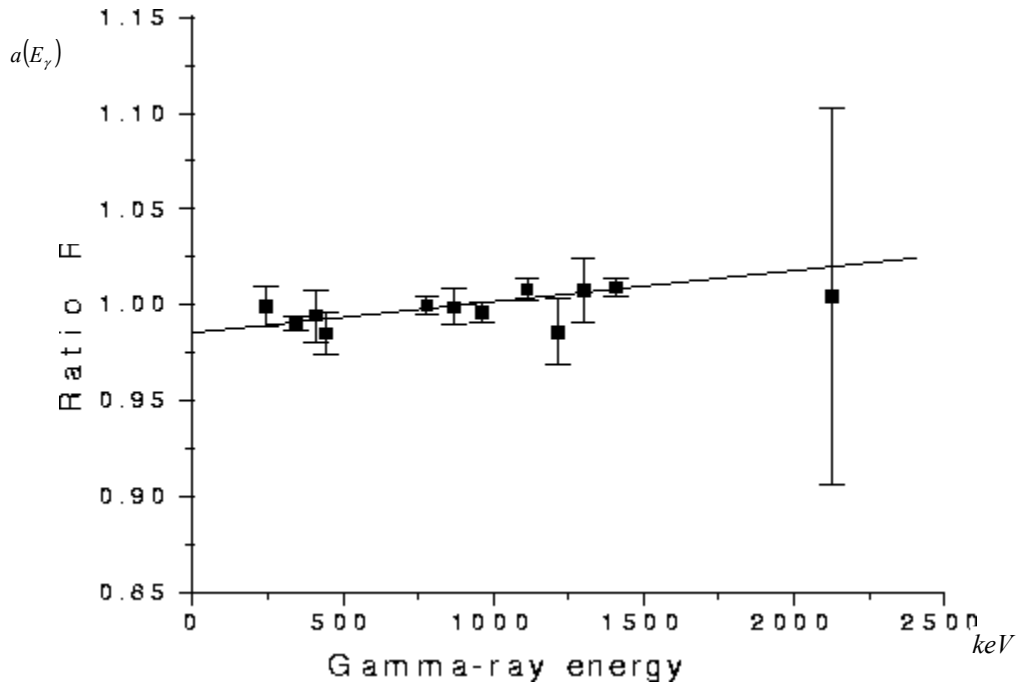


**Figure 3.7.** The figure shows the correction coefficient dependency on energy.

To determine the multipole of radiation we need to determine the  $R_{DCO}$  ratio, the angular Directional Correlations of Oriented States, which are defined as

$$R_{DCO}(158-103; \gamma_1, \gamma_2) = \frac{I(\gamma_1 \text{ at } 158^\circ; \text{gated with } \gamma_2 \text{ at } 103^\circ)}{I(\gamma_1 \text{ at } 103^\circ; \text{gated with } \gamma_2 \text{ at } 158^\circ)} \text{ in my work.}$$

In the EUROBALL detection system the germanium detectors are placed in a near-spherical shell. The detectors are situated at different angles relative to the beam axis. Therefore the system has the capability of determining the different directions of radiation. The five cluster detectors at the most backward angles are situated at  $158^\circ$ . Clover detectors are situated at  $77^\circ$  and  $103^\circ$ . Since the angular distributions and angular correlations of  $\gamma$ -rays are symmetric with respect to  $90^\circ$  (in fusion-evaporation reactions), the statistics of the two clover rings can be added together.

Fig. 3.8. shows how the multipole character of the radiation depends on the  $R_{DCO}$  ratio. The pure dipole has  $R_{DCO} \sim 0.5-0.6$ ; the pure quadrupole has  $R_{DCO} \sim 1.0$ . The transitions with other  $R_{DCO}$  values are mixed. Known stretched E2 transitions were used for gating.

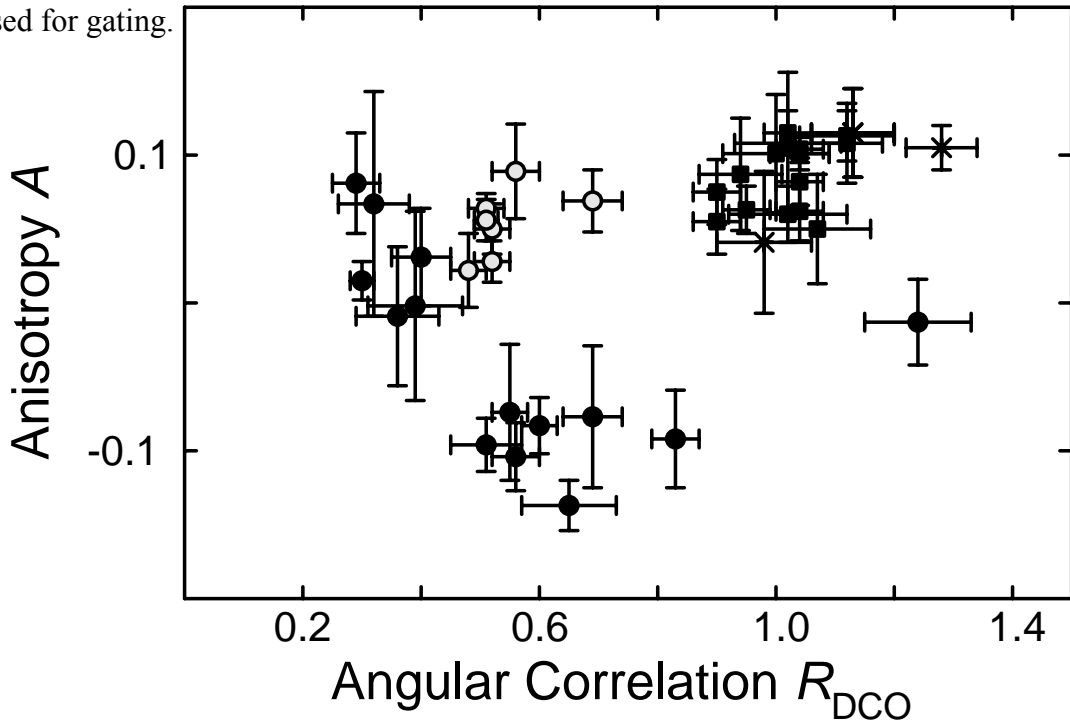


**Figure 3.8.** Anisotropy,  $A$ , and the angular correlation ratio,  $R_{DCO}$  for  $\gamma$ -rays in  $^{61}\text{Cu}$ . The open circles and filled squares denote stretched E1 and E2 transitions, respectively. Crosses denote  $\Delta I = 0$  ( $\Delta\pi = 0$ ) transitions; filled circles mixed E2/M1 or stretched M1 ( $\Delta I = 1$ ,  $\Delta\pi = 0$ ) transitions.

## 4. Results

As a result of my master thesis project the new level diagrams for  $^{60}\text{Cu}$  and  $^{61}\text{Cu}$  are obtained. By doing a  $\gamma\text{-}\gamma$  coincidence matrix (See analysis section) these two uncompleted schemes from 1982 have been extended up to a much bigger schemes with higher energy levels. This kind of analysis has been done in parallel by other members of the Nuclear Structure Group. These two energy levels diagrams are represented in Figs. 4.1. and 4.2.

The results of the polarization measurement are represented in Table 4.1.

**Table 4.1.** Energies for the excited states in the residual nuclei in the  $A=60$  mass region from the described above fusion-evaporation reaction, transition energies,  $R_{DCO}$  ratios with the error values in the brackets, asymmetry values with the errors in the brackets, multipole assignment, and spins and parities of the initial and final states. The energy levels with the previously unknown spin and parity are marked with an asterisk. Doublet structures are marked with “^a”.

Ex	Eg	Rdco (Vinkelkorr.)	A	Mult.	Ii	If
$^{60}\text{Cu}$						
62	62	-	-	-	1+	2+
287	225	0.52(9)	-0.097(27)	M1	2+	1+
	287^a	-	+0.051(33)	$\Delta I=0$	2+	2+
454	454	0.44(3)	-0.061(7)	E2/M1	3+	2+
558	104	-	-	-	4+	3+
	270	0.90(11)	+0.125(22)	E2	4+	2+
	558	1.05(7)	+0.084(6)	E2	4+	2+
781	327	-	+0.187(69)	$\Delta I=0$	3+	3+
	781	-	-	-	3+	2+
1421*	967	-	-0.047(33)	E2/M1	4+	3+
	1134	-	-	E2	4+	2+
1604	823	-	-	-	5+	3+
	1046	0.25(2)	+0.006(5)	E2/M1	5+	4+
1779	1221	0.67(1)	+0.022(30)	E2/M1	5+	4+
	1325	-	+0.073(30)	E2	5+	3+
2027	1469	-	-0.011(13)	E2/M1	5+	4+
	1573	-	+0.090(45)	E2	5+	3+
2197	594	-	-	-	6+	5+
	1640	0.94(6)	+0.060(6)	E2	6+	4+
2692	1088	0.29(6)	+0.002(17)	E2/M1	6+	5+
	1271	-	-	-	6+	4+
2817*	790	0.85(15)	-0.079(49)	E2/M1	6+	5+
3065*	2507	-	+0.136(38)	E2	6+	4+
3156	1129^a	-	+0.065(11)	E1	6-	5+
	1552	0.45(4)	+0.029(10)	E1	6-	5+
3191	994	0.50(12)	-	M1	7+	6+
	1411	-	-	-	7+	5+
	1587	0.95(14)	+0.071(17)	E2	7+	5+

3354	1157	0.49(3)	+0.051(5)	E1	7-	6+
3745*	928	-	-0.150(117)	E2/M1	7+	6+
	1718	-	-	-	7+	5+
3772	417	1.00(10)	+0.126(12)	deltaI=0	7-	7-
	616^a	0.60(12)	-0.047(17)	M1	7-	6-
4004*	1977	-	+0.044(42)	E1	6-	5+
4074*	1382	-	+0.045(43)	(E2)	(8+)	6+
4290*	286^a	0.68(6)	-0.080(29)	E2/M1	7-	6-
	1134	0.46(11)	-0.070(28)	M1	7-	6-
	1225	-	-	-	7-	6+
	1474	-	-	-	7-	6+
	1598	-	-	-	7-	6+
4521*	1166	0.23(5)	+0.026(18)	E2/M1	8-	7-
	1330	0.46(8)	+0.039(19)	E1	8-	7+
	1365	0.96(13)	+0.086(15)	E2	8-	6-
4580*	835	-	-	-	(8+)	7+
	1763	-	+0.141(113)	(E2)	(8+)	6+
4816*	525	-	-0.085(38)	M1	8-	7-
	1462	-	-	-	8-	7-
	1625	-	-	-	8-	7+
4843	552	0.78(6)	-0.069(13)	E2/M1	8-	7-
	1488	-	-	-	8-	7-
5188	667^a	-	-	-	9-	8-
	1416	1.03(12)	+0.060(19)	E2	9-	7-
	1833	1.15(17)	+0.054(16)	E2	9-	7-
5247	667^a	-	-	-		(8+)
	1501	-	-	-		7+
	2056	-	-	-		7+
5434*	591	0.80(5)	-0.089(16)	E2/M1	9-	8-
	618^a	-	+0.013(27)	M1	9-	8-
5648*	461	0.50(6)	-0.084(11)	M1	10-	9-
	1128^a	0.99(8)	+0.070(9)	E2	10-	8-
5862*	1342	0.58(12)	+0.074(49)	E1	9+	8-
	2672	-	-	-	9+	7+
6009*	2818	-	-	E2	9+	7+
6076*	643	0.85(5)	-0.035(13)	E2/M1	10-	9-
6094*	446	0.38(8)	-0.019(19)	E2/M1	11-	10-
	906	0.90(11)	+0.075(18)	E2	11-	9-
6852*	775	0.75(5)	-0.090(18)	E2/M1	11-	10-
7394*	1386	-	+0.194(54)	E2	11+	9+
	1532	0.99(10)	+0.074(24)	E2	11+	9+
	1746	0.51(4)	+0.046(8)	E1	11+	10-
8132*	738	1.05(6)	+0.099(6)	E2	13+	11+
	2038	1.19(32)	-0.136(46)	M2	13+	11-
61Cu						
970	970	0.30(2)	+0.015(13)	E2/M1	5/2-	3/2-
1310	340	0.56(4)	-0.104(23)	M1	7/2-	5/2-
	1310	1.04(4)	+0.104(9)	E2	7/2-	3/2-
1394	1394	-	-	-	5/2-	3/2-
1733	338	-	-	-	7/2-	5/2-
	422	1.28(6)	+0.105(15)	deltaI=0	7/2-	7/2-
	762	-	-0.154(37)	M1	7/2-	5/2-
	1733	1.04(4)	+0.062(20)	E2	7/2-	3/2-
1942	210	-	-	-	7/2-	7/2-
	632^a	1.13(7)	+0.115(30)	deltaI=0	7/2-	7/2-

	972	-	-0.044(24)	M1	7/2-	5/2-
	1942	-	-	-	7/2-	3/2-
2295	338	-	-	-	9/2-	7/2-
	562 <sup>a</sup>	-	-	-	9/2-	7/2-
	901	-	-	-	9/2-	5/2-
	985	0.83(4)	-0.092(33)	E2/M1	9/2-	7/2-
	1325	-	+0.158(64)	E2	9/2-	5/2-
2336	1026	0.40(5)	+0.031(33)	E2/M1	9/2-	7/2-
	1366	-	+0.110(18)	E2	9/2-	5/2-
2612	670	-	-0.064(28)	M1	9/2-	7/2-
	880	1.24(9)	-0.013(29)	E2/M1	9/2-	7/2-
2627	1316	1.04(4)	+0.082(16)	E2	11/2-	7/2-
2721	988	0.52(3)	+0.050(17)	E1	9/2+	7/2-
	1410	0.51(3)	+0.064(10)	E1	9/2+	7/2-
3016	679	0.36(7)	-0.009(47)	E2/M1	11/2-	9/2-
	721	0.49(9)	-	-	11/2-	9/2-
	1705 <sup>a</sup>	0.90(4)	+0.055(22)	E2	11/2-	7/2-
3260	633 <sup>a</sup>	1.13(7)	+0.115(30)	deltaI=0	11/2-	11/2-
	648 <sup>a</sup>	0.55(3)	-0.076(46)	E2/M1	11/2-	9/2-
	1527	1.02(9)	+0.108(48)	E2	11/2-	7/2-
3548	922	0.98(8)	+0.041(48)	deltaI=0	11/2-	11/2-
	936	0.69(5)	-0.077(48)	M1	11/2-	9/2-
	1253	-	-	-	11/2-	9/2-
	1606	-	-	-	11/2-	7/2-
3780	1444 <sup>a</sup>	1.07(9)	+0.050(37)	E2	13/2-	9/2-
3943	1222	0.32(6)	+0.067(76)	E2/M1	11/2+	9/2+
3970*	710	-	-	-	13/2-	11/2-
	1343	0.29(4)	+0.081(34)	E2/M1	13/2-	11/2-
	1358	-	-	-	13/2-	9/2-
4053	1717	-	-	-	13/2-	9/2-
4082	1065	0.52(3)	+0.028(14)	E1	13/2+	11/2-
	1361	1.02(4)	+0.115(15)	E2	13/2+	9/2+
4287	1951	1.00(9)	+0.101(40)	E2	13/2-	9/2-
	1992	-	-	-	13/2-	9/2-
4468	1841	0.94(7)	+0.087(38)	E2	15/2-	11/2-
4591	648 <sup>a</sup>	0.55(3)	-0.076(46)	E2/M1	13/2+	11/2+
	1042	0.48(3)	+0.022(25)	E1	13/2+	11/2-
	1330	0.69(5)	+0.069(21)	E1	13/2+	11/2-
	1870	1.12(6)	+0.108(27)	E2	13/2+	9/2+
4820*	766	-	-	-	15/2-	13/2-
	849 <sup>a</sup>	-	-	-	15/2-	13/2-
	1559	-	-	-	15/2-	11/2-
	2193	-	-	-	15/2-	11/2-
4991*	909	0.39(8)	-0.002(64)	E2/M1	15/2+	13/2+
	1048	-	-	-	15/2+	11/2+
5120	300	0.55(4)	-	E1	17/2+	15/2-
	529	1.04(5)	+0.101(11)	E2	17/2+	13/2+
	652	0.56(4)	+0.089(32)	E1	17/2+	15/2-
	1038	0.95(4)	+0.063(16)	E2	17/2+	13/2+
5137*	850 <sup>a</sup>	0.70(9)	-	E2/M1	15/2-	13/2-
5580*	1800	-	-	-	-	13/2-
5702*	565 <sup>a</sup>	-	+0.179(25)	-	15/2+	15/2-
	582	-	+0.160(45)	-	15/2+	15/2-
	1414	-	+0.127(43)	E1	15/2+	13/2-
	1731 <sup>a</sup>	-	-	-	15/2+	13/2-
5729*	592	-	-	-	15/2	15/2-
	1442 <sup>a</sup>	-	-	-	15/2	13/2-

	1647	-	-	-		15/2	13/2+
5856*	736	0.65(8)	-0.137(17)	M1		19/2+	17/2+
6056*	327	0.65(5)	-	delta I=1		17/2+	15/2+
	354	0.60(3)	-0.083(19)	M1		17/2+	15/2+
	1236	-	-	-		17/2+	15/2-
	1974	-	-	-		17/2+	13/2+
6572*	516	0.51(6)	-0.096(18)	M1		19/2+	17/2+
	1452	-	-	E2/M1		19/2+	17/2+
6824	968 <sup>a</sup>	-	-	-		21/2+	19/2+
	1704	0.90(4)	+0.075(22)	E2		21/2+	17/2+
7389*	564 <sup>a</sup>	0.57(6)	-	M1		23/2+	21/2+
	1532	1.02(10)	+0.060(19)	E2		23/2+	19/2+
7937*	1112	0.51(2)	+0.056(14)	E1		23/2-	21/2+
9408*	1472	1.12(8)	+0.113(17)	E2		27/2-	23/2-
56Co							
577	577	0.62(3)	-0.055(9)	M1		5+	4+
2283	1706	-	+0.060(9)	E2		7+	5+
3637	1355	1.24(7)	-0.086(14)	E2/M1		8+	7+
4179	542	0.57(4)	-0.165(39)	E2/M1		9+	8+
	1897	1.11(6)	+0.031(14)	E2		9+	7+
5273	1094	0.68(4)	-0.046(16)	E2/M1		10+	9+
57Co							
1224	1224	0.77(4)	-0.049(9)	E2/M1		9/2-	7/2-
1690	466	0.56(3)	-0.077(4)	M1		11/2-	9/2-
	1690	0.98(5)	+0.061(12)	E2		11/2-	7/2-
2524	834	0.65(3)	-0.052(4)	M1		13/2-	11/2-
4036	1512	-	-0.072(21)	M1		15/2-	13/2-
4813	2290	0.99(5)	+0.065(7)	E2		17/2-	13/2-
4845	3155	0.56(4)	+0.032(10)	E1		13/2+	11/2-
5434	589	0.80(4)	-0.058(5)	E2/M1		15/2+	13/2+
5755	321	0.56(3)	-0.093(7)	M1		17/2+	15/2+
5918	1104	0.84(4)	-0.051(6)	E2/M1		19/2-	17/2-
6517	762	0.63(4)	-0.068(8)	E2/M1		19/2+	17/2+
6975	1058	0.78(4)	-0.041(9)	E2/M1		21/2-	19/2-
58Ni							
1454	1454	1.00(4)	+0.065(5)	E2		2+	0+
2459	1005	1.07(5)	+0.068(4)	E2		4+	2+
3620	1161	1.11(5)	+0.070(5)	delta I=0		4+	4+
	2166	1.03(6)	+0.044(22)	E2		4+	2+
4382	763	0.89(7)	-0.096(4)	M1		5+	4+
	1924	0.22(1)	+0.013(8)	E2/M1		5+	4+
5128	745	0.73(3)	-0.091(5)	E2/M1		6+	5+
	2668	0.95(4)	+0.056(10)	E2		6+	4+
5383*	1001	-	-0.010(15)	E2/M1		6+	5+
6066	683	0.46(3)	-0.083(19)	E2/M1		7+	5+
	939	0.83(4)	-0.072(5)	E2/M1		7+	6+
6083*	700	0.46(4)	+0.039(19)	E1		7-	6+
	956	0.59(3)	+0.054(15)	E1		7-	6+
	3624	1.84(24)	+0.080(78)	E3		7-	4+
6603	384	0.55(8)	-0.137(54)	M1		8+	7+
	537	0.68(3)	-0.084(4)	M1		8+	7+

	1476	1.12(5)	+0.072(7)	E2	8+	6+
7273*	2146	0.48(15)	+0.048(30)	E1	7-	6+
7445	842 <sup>a</sup>	-	-	M1	9+	8+
8113*	709	-	-0.119(11)	M1	8-	7-
8120*	1517	0.67(5)	-0.023(10)	E2/M1	9+	8+
8716*	735	0.76(8)	-0.106(16)	M1	9-	8-
	2113	-	+0.079(21)	E1	9-	8+
9344	628	0.65(3)	-0.066(8)	E2/M1	10-	9-
10179	835 <sup>a</sup>	0.73(3)	-0.058(4)	E2/M1	11-	10-
11253	560	0.61(4)	-0.154(33)	M1	11-	10-
13235	668	0.67(4)	-0.056(19)	M1	13+	12+
14125	890	0.72(5)	-0.124(15)	M1	14+	13+
59Ni						
339	339	0.58(3)	-0.121(15)	M1	5/2-	3/2-
1337	998	0.99(5)	-0.007(13)	E2/M1	7/2-	5/2-
1767	429	-	-0.056(27)	M1	9/2-	7/2-
	1428	0.88(8)	+0.062(8)	E2	9/2-	5/2-
1947	1609 <sup>a</sup>	0.53(5)	-0.044(13)	M1	7/2-	5/2-
2704	1367	0.94(5)	+0.067(9)	E2	11/2-	7/2-
3054	1106	0.52(3)	+0.028(30)	E1	9/2+	7/2-
	1717	0.57(5)	+0.045(26)	E1	9/2+	7/2-
3375	671 <sup>a</sup>	0.96(7)	-0.006(25)	deltaI=0	11/2-	11/2-
	1609 <sup>a</sup>	0.61(4)	-0.041(14)	M1	11/2-	9/2-
3558	854	1.15(9)	+0.051(23)	deltaI=0	11/2-	11/2-
	1792	0.71(6)	-0.055(31)	E2/M1	11/2-	9/2-
4102	2335	0.43(5)	-0.057(42)	E2/M1	11/2-	9/2-
4139	581	0.85(5)	-0.073(14)	E2/M1	13/2-	11/2-
	764 <sup>a</sup>	0.76(8)	-0.066(13)	E2/M1	13/2-	11/2-
4454	1401	1.04(6)	+0.080(19)	E2	13/2+	9/2+
	1750	0.48(3)	+0.013(15)	E1	13/2+	11/2-
4945	806	-	-0.075(16)	M1	15/2-	13/2-
5250	796	0.99(5)	+0.108(25)	E2	17/2+	13/2+
60Ni						
1332	1332	1.01(4)	+0.068(5)	E2	2+	0+
2506	1173	0.98(4)	+0.073(5)	E2	4+	2+
2626	467	0.74(5)	-0.045(26)	E2/M1	3+	2+
	1293	0.66(7)	-0.134(54)	M1	3+	2+
3120	1787	0.88(5)	+0.053(14)	E2	4+	2+
3671	1165	0.99(6)	+0.086(15)	deltaI=0	4+	4+
4165	1660	0.20(2)	-0.002(21)	E2/M1	5+	4+
4265	1145	1.03(8)	+0.072(30)	E2	6+	4+
	1759	1.02(5)	+0.070(6)	E2	6+	4+
4986	1315	-	+0.036(35)	E2	6+	4+
	2480	0.96(5)	+0.053(22)	E2	6+	4+
5014	1894	0.41(3)	+0.047(36)	E1	5-	4+
	2507	0.46(5)	+0.053(27)	E1	5-	4+
5348	334	0.93(4)	+0.113(17)	E2	7-	5-
	363	0.51(3)	+0.092(19)	E1	7-	6+
	1083	0.48(2)	+0.046(4)	E1	7-	6+
	2842	1.31(17)	+0.122(74)	E3	7-	4+
5663	677	0.80(4)	-0.101(14)	E2/M1	7+	6+
	1398	0.45(4)	-0.062(24)	M1	7+	6+
6461	798	0.78(11)	-0.110(15)	E2/M1	8+	7+

6811	1462 <sup>a</sup>	-	+0.052(9)	E2	9-	7-
6837	1488	1.43(8)	-0.086(15)	E2/M1	8-	7-
8044	284	0.41(4)	-0.162(35)	M1	9-	8-
	353	0.46(3)	-0.135(26)	M1	9-	8-
	1207	0.80(19)	-0.088(18)	E2/M1	9-	8-
	2696	0.95(8)	+0.032(32)	E2	9-	7-
8272	1461 <sup>a</sup>	-	+0.009(12)	E2/M1	10-	9-
8521	1710	0.78(6)	-0.029(12)	E2/M1	10-	9-
	2696	0.95(8)	+0.032(32)	E2	9-	7-
9133	612	0.68(3)	-0.064(6)	E2/M1	11-	10-
9990	857	0.86(5)	-0.086(5)	E2/M1	12-	11-
60Zn						
1004	1004	1.11(8)	+0.063(34)	E2	2+	0+
2193	1189	0.97(7)	+0.091(36)	E2	4+	2+
3808	1615	1.04(8)	-	E2	6+	4+
61Zn						
124	124	0.38(3)	-	E2/M1	5/2-	3/2-
996	873	0.30(4)	+0.041(12)	E2/M1	7/2-	5/2-
	996	0.99(6)	+0.071(62)	E2	7/2-	3/2-
1265	1141	1.15(9)	+0.096(25)	E2	9/2-	5/2-
2270	1273	-	+0.096(38)	E2	11/2-	7/2-
2399*	1403	0.54(4)	+0.063(13)	E1	9/2+	7/2-
2797	1532	0.91(7)	+0.027(75)	E2	13/2-	9/2-
3336	937	1.11(7)	+0.087(12)	E2	13/2+	9/2+
	1066	0.45(6)	+0.138(52)	E1	13/2+	11/2-
4264	1467	0.44(4)	+0.074(31)	E1	15/2+	13/2-
4415	1079	0.99(6)	+0.072(14)	E2	17/2+	13/2+
4645	1849	1.00(12)	+0.122(54)	E2	17/2-	13/2-
5553	1289	0.88(7)	+0.103(30)	E2	19/2+	15/2+
6090	1675 <sup>a</sup>	0.91(6)	+0.059(20)	E2	21/2+	17/2+
7486	1396	0.94(7)	+0.094(69)	E2	25/2+	21/2+
7629	1538	0.48(3)	+0.090(17)	E1	23/2-	21/2+
9162	1533	0.95(7)	+0.039(22)	E2	27/2-	23/2-
	1676 <sup>a</sup>	-	-	E1	27/2-	25/2+
10156	994 <sup>a</sup>	0.99(6)	+0.125(36)	E2	31/2-	27/2-
* Level with previously unknown spin and parity.						
a Doublet structure.						

The level schemes used in the analysis were taken from Refs. [10,11] ( $^{60}\text{Cu}$ ), [12,13] ( $^{61}\text{Cu}$ ), [14] ( $^{56}\text{Co}$ ), [15] ( $^{57}\text{Co}$ ), [12,16] ( $^{58}\text{Ni}$ ), [17,18] ( $^{59}\text{Ni}$ ), [19] ( $^{60}\text{Ni}$ ), [20] ( $^{60}\text{Zn}$ ), and [12,21] ( $^{61}\text{Zn}$ ).

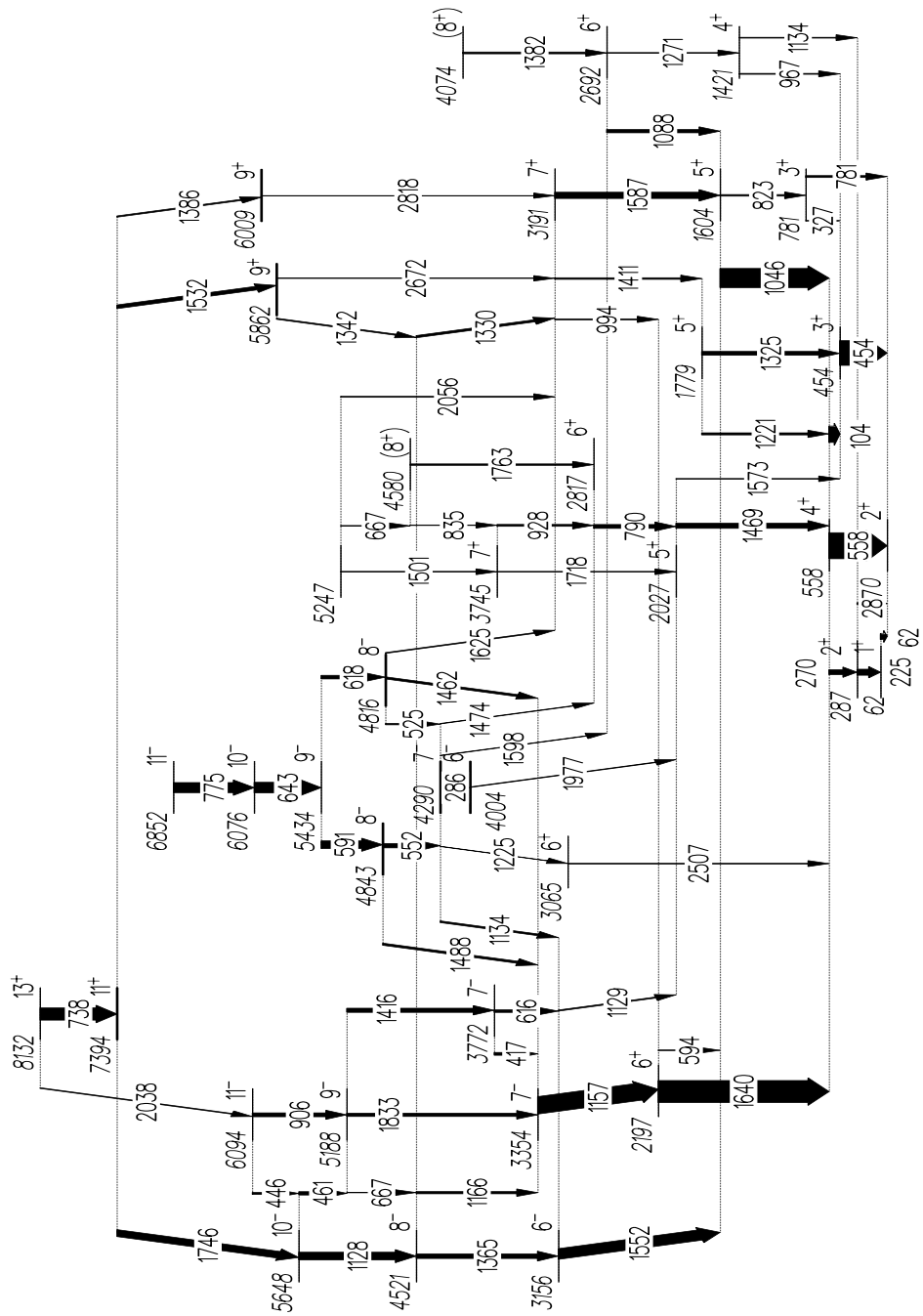
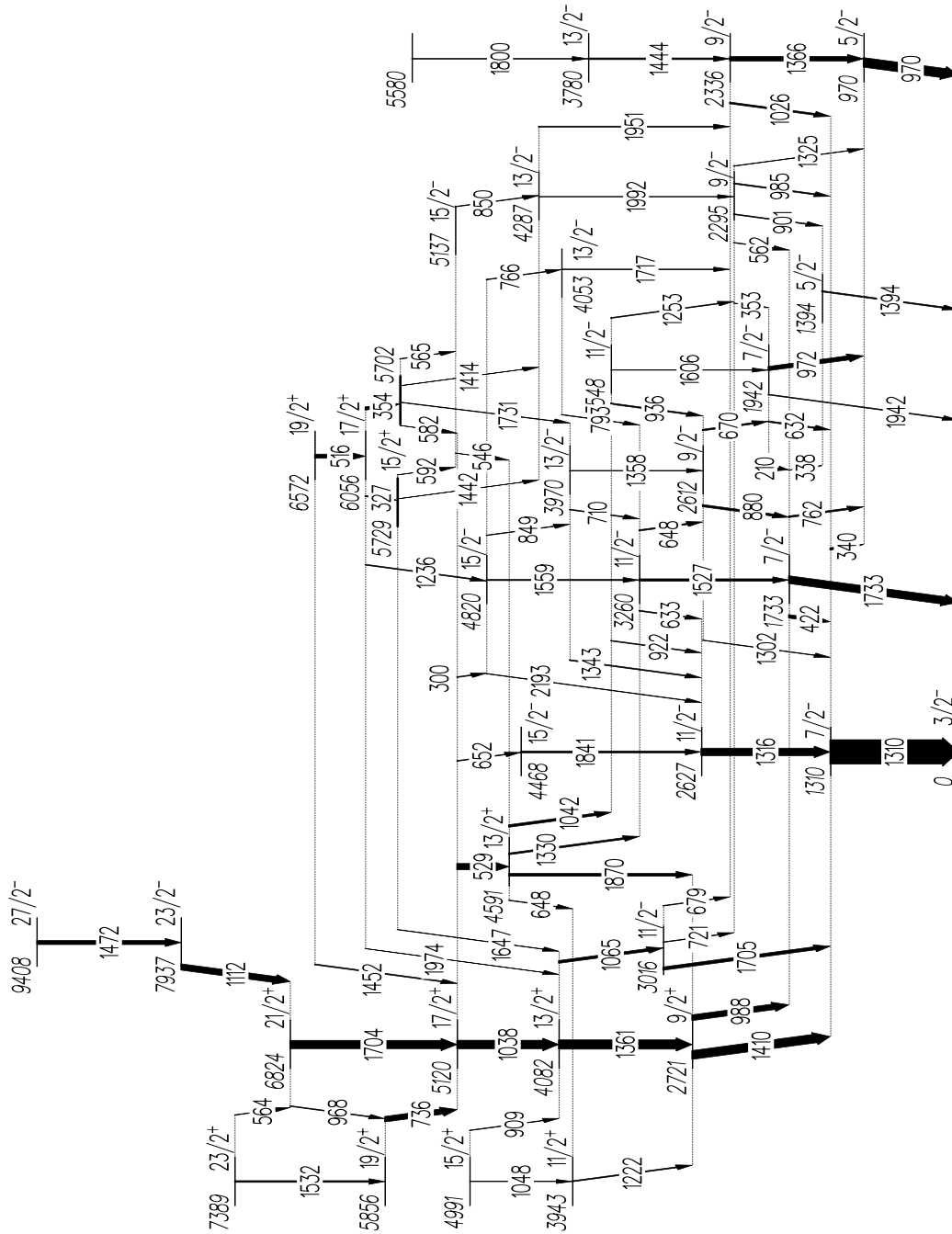


**Figure 4.1.** The proposed level scheme of  $^{60}\text{Cu}$ . The width of the arrows corresponds to the relative intensities of the transitions. The tentative numbers are given in parentheses.



## 5. DISCUSSION

The aim of my master degree thesis was to measure the polarization in various residual nuclei, which were populated in the fusion-evaporation reaction  $^{24}\text{Mg}(^{40}\text{Ca},x\text{pyn}\alpha)$ . The polarization measurements have supported most of the spin and the parity values from the existing schemes [10-21]. In addition, uncertain values of spin and parity have been corrected. Totally I have analyzed 13 nuclei, but not all of them are reported in my work. For instance, the channels  $^{58}\text{Cu}$  and  $^{59}\text{Cu}$  are too weak to get reasonable asymmetry values. The most suitable nuclei for discussion are  $^{60}\text{Cu}$  and  $^{61}\text{Cu}$  because their energy level diagrams contains several transitions, which are interesting for the discussion.

I will start this section with the discussion of  $^{60}\text{Cu}$ . During my master thesis project I have used a level scheme of  $^{60}\text{Cu}$  taken from [10] from 1982. This level scheme is incomplete and the highest excitation energy is 5188 keV with the spin and the parity  $I=9^-$ . In addition, it is unclear which spin and parity some levels have. After the polarization measurements some new transitions were placed in the proposed level scheme shown in Fig. 4.1. It was extended up to an excitation energy of 8132 keV with the spin and the parity  $I=13^+$ . Unknown spins and parities were determined with the help of asymmetry values and the following selections rules for angular momentum and parity taken from [4]

$$|I_i - I_f| \leq L \leq |I_i + I_f| \quad (\text{no } L=0)$$

$$\begin{array}{ll} \Delta\pi = \text{no} & \text{even electric } L, \text{ odd magnetic } L \\ \Delta\pi = \text{yes} & \text{odd electric } L, \text{ even magnetic } L \end{array}$$

For instance, it was unclear which spin,  $I=3^+$  or  $I=4^+$ , the 1421 keV level should be ascribed. The asymmetry value shows that the transition of 967 keV ( $3^+ \rightarrow 4^+$ ) has mixed multipolarity, E2/M1, without change in parity ( $\Delta\pi = \text{no}$ ). From the theory we know that the emission of E2 is less probable than the emission of M1 by factor of  $10^{-3}$  [2] and  $\Delta I \geq 3$  transitions are generally excluded. So we can approximate that this emission is mainly magnetic with  $L=1$ . This leads to the conclusion that the level 1421 keV has spin  $I=3^+$ . In the same way the parity of the 2817 keV level can be calculated. The transition of 791 keV is E2/M1. The emission of M1 is most probable like in the previous example, so the lowest possible multipole is M1 therefore  $L=1$ . According to the selections rules above, there is no change in parity ( $\Delta\pi = \text{no}$ ), so the level of 2817-keV has spin and parity  $6^+$ . After the polarization measurements the spin and the parity of the 3065 keV level can be calculated. The asymmetry value and the  $R_{DCO}$  ratio show that the multipolarity of the 2509 keV line is E2. The even electric transition ( $L=2$ ) and no change in parity ( $\Delta\pi = \text{no}$ ) shows that the level of 3065 keV has spin  $I=6^+$ . The same calculations can be done with the 1166 keV line, which is a mixture of E2/M1. The lowest multiple transition is M1 ( $L=1$ ). It follows that the level 4521 keV has spin  $I=8^-$ .

The level scheme of  $^{61}\text{Cu}$  I used in my work was also incomplete with the highest excitation energy of 9408 keV and unknown spin and parity for this level. With the help of the shell model calculations, the energy spectra from the experiment and polarization measurements some new transitions were placed in the proposed scheme shown in the figure 4.2.

Another interesting example I can describe here is how one can indirectly determine the spin and the parity of some levels without known asymmetry value. The 4820 keV level has uncertain spin and parity in the level scheme taken from [6]. It was not possible to obtain the asymmetry values for 766-, 849-, 1559-, and 2193-keV transitions as shown in the result table. Neither has the 300 keV line between the 5120 keV and 4820 keV levels an asymmetry value. But we know that the 3260 keV level has spin  $I=11/2^-$  while the 5120 keV level has spin  $I=17/2^+$ . According to theory, only the multipolarities E1, M1, and E2 can occur. The  $R_{DCO}$  value, which is 0.55, shows that the 300 keV line is pure dipole, i.e. either E1 or M1. If it is M1 the 4820 keV level should have spin  $I=15/2^+$  according to the selections rules. It follows from this that the 1559 keV line is pure M2, which is excluded according to the theory. It means that the 300 keV transition is pure E1 which results that the 4820 keV level has spin  $I=15/2^-$ . By the calculations of radiation character for 1559 keV transition we can control our conclusions. For the 1559 keV line  $L = 2$  and  $\Delta\pi = no$ , which means that it is a pure E2, and this is possible according to the theory.

With the help of the asymmetry values and the  $R_{DCO}$ , the spin and the parity of some other lines have been calculated in the  $^{61}\text{Cu}$  energy level scheme namely 1942-( $7/2^-$ ), 3260-( $11/2^-$ ), 3780-( $13/2^-$ ), 4990-( $15/2^+$ ), 5138-( $15/2^-$ ), 5703-( $15/2^+$ ), 5856-( $19/2^+$ ), 6056-( $17/2^+$ ), 6825-( $21/2^+$ ), 7389-( $23/2^+$ ), 7937-( $23/2^-$ ), 9408 keV ( $27/2^-$ ) etc.

$^{61}\text{Cu}$  consists of 29 protons and 32 neutrons. From the shell model we know that when a nucleus has either a major proton or neutron energy level filled, it is more stable than the energy level with unpaired nucleons. The extreme limit of the shell model asserts that 32 neutrons fill all orbitals including the  $2p_{3/2}$  orbital and pairwise couple to zero spin. According to the shell model only the single unpaired valence proton at the  $2p_{3/2}$  energy level determines the properties of the ground state of  $^{61}\text{Cu}$ . The 29th proton is outside of the close shell with a magic number 28. A shell is defined as several energy levels lying close together, clearly separated from other shells. Magic numbers represent the closing of a shell. The nuclei with magic numbers are very stable since the energy gap to the next shell is large.

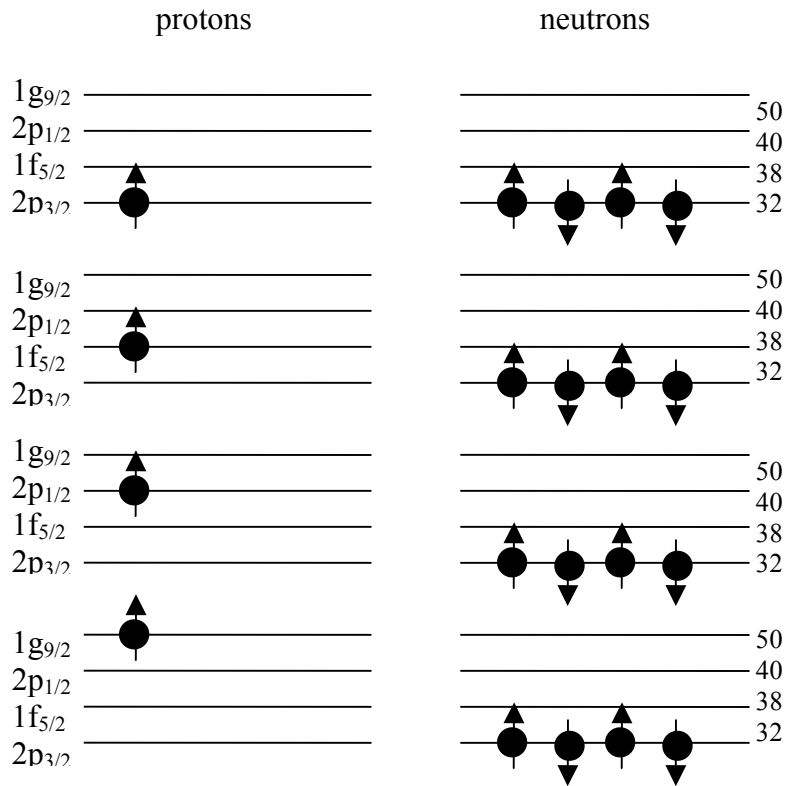


**Figure 5.1.** Proton and neutron configurations in  $^{61}\text{Cu}$ . The valence proton can occupy four different orbital:  $2p_{3/2}$ ,  $1f_{3/2}$ ,  $2p_{1/2}$ ,  $1g_{9/2}$ . The four valence neutrons are in the lowest orbital  $2p_{3/2}$ . The black dots illustrate the nucleons; the white dots mark the holes.

Quantum mechanically every nucleon can be labeled with the corresponding quantum numbers  $n$ ,  $l$ ,  $j$ ,  $m_j$ , where  $n$  is a radial quantum number,  $l$  is orbital angular momentum,  $j$  is total angular momentum, and  $m_j$  is projection of the total angular momentum on the  $z$ -axis. The notation for the orbital angular momentum is  $s$  for  $l=0$ ,  $p$  for  $l=1$ ,  $d$  for  $l=2$ ,  $f$  for  $l=3$ ,  $g$  for  $l=4$ . In the shell model the parity of the orbital is given by  $\pi = (-1)^l$  and the resulting parity of a nucleus in a certain state is the product according to

$$\pi = \prod_{i=1}^A \pi_i = \prod_{i=1}^A (-1)^{l_i} .$$

We can consider the energy levels in the fifth shell because it is relatively easy to excite the single protons to these levels. There are four possible ways to place the single unpaired proton in these orbits, i.e. four possible configurations. They are shown in Fig. 5.1.

On the energy level diagram (see Fig. 4.2.) we can find three levels with spin and parity shown above, namely 0 keV( $3/2^-$ ), 970 keV( $5/2^-$ ), 2721 keV( $9/2^+$ ). The proton can be excited in a sequence 0 keV( $3/2^-$ ) -970 keV( $5/2^-$ ) - 2721 keV( $9/2^+$ ). There is not a level with the spin and parity  $I^\pi=1/2^-$  in the level diagram. This low-spin state is not populated in the present reaction.

The neutrons can also be excited. In the ground state all the four neutrons are in the  $2p_{3/2}$  orbital. If one neutron excites to the  $1f_{5/2}$  level than the maximum value of the total angular momentum of the all four neutrons is  $3/2+1/2-1/2+5/2=8/2=4$  due to the neutrons are fermions and obey the Pauli principle. The maximum value of the nuclear total angular momentum can be  $I=3/2+8/2=11/2$  if the unpaired proton has the spin  $3/2^-$ . And then the nucleus will be excited by the sequence 0 keV( $3/2^-$ )-1310 keV( $7/2^-$ )-2627 keV( $11/2^-$ ). The unpaired proton and unpaired neutrons in this state have  $l$ -values 1 and 3. The resultant parity is  $\pi = (-1)^1(-1)^1(-1)^3 = -1$ , i.e. negative.

If the unpaired proton has the spin  $5/2^-$  than the nuclear total angular momentum can be  $I=5/2+8/2=13/2$  and the nucleus can be excited in the following way 970 keV( $5/2^-$ )-2336 keV( $9/2^-$ )-3780 keV( $13/2^-$ ). The resultant parity is  $\pi = (-1)^3(-1)^1(-1)^3 = -1$ , i.e. negative.

If the excited proton occupies the  $9/2^+$  level then  $I=9/2+8/2=17/2$  and the way of the excitation is 2721 keV( $9/2^+$ )-4082 keV( $13/2^+$ )-5120 keV( $17/2^+$ ) and the resultant parity is  $\pi = (-1)^4(-1)^1(-1)^3 = 1$ , i.e. positive parity (See Fig. 5.2.).

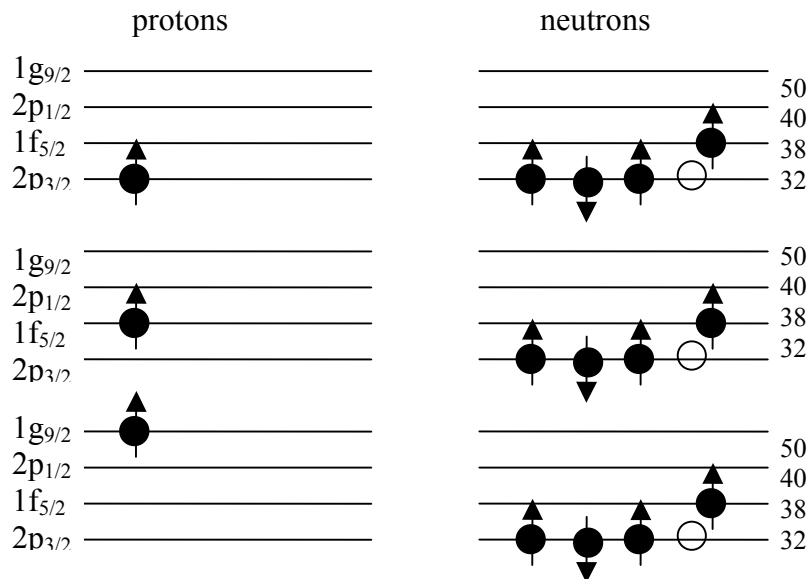


**Figure 5.2.** Valence proton and the valence neutrons in the fifth shell of  $^{61}\text{Cu}$ . The valence proton is in the three different modes:  $2p_{3/2}$ ,  $1f_{5/2}$ ,  $1g_{9/2}$ . The three of the four valence neutrons are on the  $2p_{3/2}$  energy level and the fourth neutron is on the  $1f_{5/2}$  energy level.

If the energy is enough than two neutrons can be excited from the  $2p_{3/2}$  to the  $1f_{5/2}$  level (See Fig. 5.3.). The maximum value of the total angular momentum for each neutron in the  $2p_{3/2}$  is  $j=3/2$ . But neutrons are fermions and obey the Pauli principle. Therefore only the one neutron in the  $2p_{3/2}$  level can have total angular momentum  $3/2$ . The other one has the maximum value of the total angular momentum  $1/2$ . In the same way only one of the neutrons in the  $1f_{5/2}$  level can have the maximum value of the total angular momentum  $5/2$ . According to the Pauli principle the other neutron in the  $1f_{5/2}$  level has the maximum value of the total angular momentum  $3/2$ . The maximum value of the total angular momentum for all four neutrons is  $5/2+3/2+3/2+1/2=12/2=6$ .

The coupling to spin 6 of the four unpaired neutrons to a proton in the  $2p_{3/2}$ ,  $1f_{5/2}$ , or  $1g_{9/2}$  orbital gives rise to the 4468 keV( $15/2^-$ ), 5580 keV ( $17/2^-$ ), and 6824 keV( $21/2^+$ ) states, respectively.

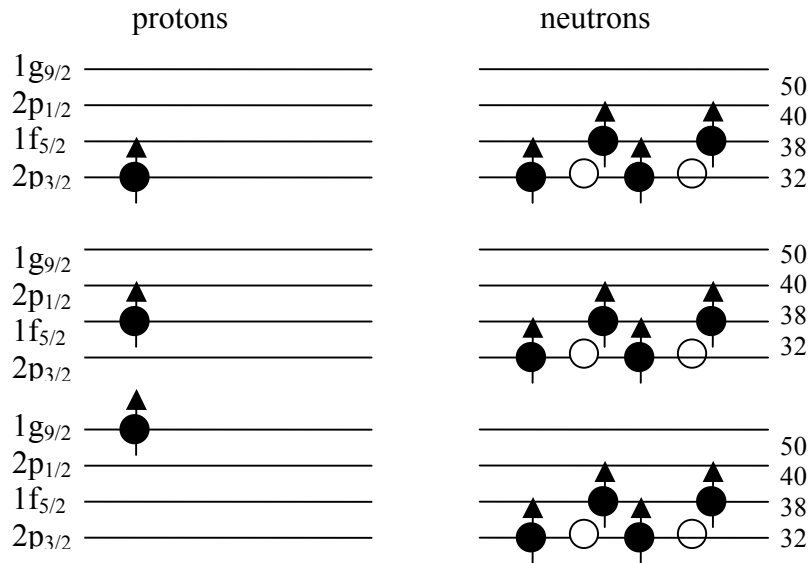


**Figure 5.3.** Valence proton and neutrons in the different modes in the fifth shell of  $^{61}\text{Cu}$ .

The parity changes at the 1112 keV transition from 6824 keV( $21/2^+$ ) to 7937 keV( $23/2^-$ ) level. It can be explained with the help of the shell model. One of the neutrons is excited from one level to another level with the opposite parity. For instance, the proton is excited to the  $1g_{9/2}$  level, resulting in  $9/2^+$  state. The neutrons have the following positions: two neutrons are in the  $2p_{3/2}$  orbit and couple to spin 0. They do not contribute to the structure. The other two neutrons are in the  $1f_{5/2}$  and  $1g_{9/2}$  orbits, respectively as shown in Fig. 5.3. The maximum value of the neutrons total angular momentum is  $5/2+9/2=14/2=7$ . The total angular momentum of this configuration is  $9/2+14/2=23/2$  and the parity is  $\pi = (-1)^4(-1)^3(-1)^4 = -1$ , i.e. negative.

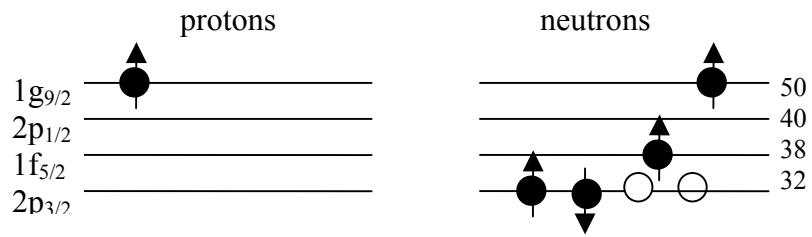


**Figure 5.4.** Valence proton and neutrons in the excited the  $23/2^-$  level in  $^{61}\text{Cu}$ .

## Acknowledgments

I would like to thank the members of the Nuclear Structure Group in Lund for their contributions in the development of my work.

I am grateful to my supervisor Dirk Rudolph for his very professional guidance during the promotion of my master thesis project. He provided me with much useful reference material and worked hard to improve the text of my composition with very detailed and useful comments.

I also thank professor Claes Fahlander for his interest in my work and encouragement he provided.

I am truly grateful to Jörgen Ekman for his help and advice during my analysis work. His friendly and patient way to answer all my questions helped me to get my master thesis project started and made many parts of my work much easier than they might have been.

OLGA IZOTOVA  
Lund, 2003.

## References

- [1] H. Benson, *University physics*, John Wiley & Sons, 1991.
- [2] J. Jackson, *Classical electrodynamics*, Wiley & Sons, 1962.
- [3] E. Hecht, *Optics*, Addison-Wesley publishing company, 1988.
- [4] K. S. Krane, *Introductory nuclear physics*, John Wiley & Sons, 1988.
- [5] G. J. Schmid *et al.*, Nucl. Instr. and Meth. in Phys. Res. A **417** (1998) 95-110.
- [6] P. M. Jones *et al.*, Nucl. Instr. and Meth. in Phys. Res. A **362** (1995) 556-560.
- [7] L. E. Berglund, *Excited States in  $^{103}\text{Sn}$* , Master Thesis, Lund University, 2000.
- [8] Gammasphere Users Executive Committee, *Gammasphere The Beginning...1993-97*.
- [9] EUROBAL III, A European  $\gamma$ -ray facility, eds. J. Gerl and R.M. Lieder, GSI 1992.
- [10] T. U. Chan *et al.*, Phys. Rev. C **26**, (1982) 434.
- [11] D. Rudolph, priv. comm..
- [12] S. M. Vincent *et al.*, Phys. Rev. C **60**, (1999) 064308.
- [13] D. Rudolph, priv. comm..
- [14] M. Palacz *et al.*, Nucl. Phys. A **627** (1997) 162-174.
- [15] O. L. Caballero *et al.*, Phys. Rev. C **67**, (2003) 024305.
- [16] D. Rudolph, priv. comm..
- [17] S. Juutinen *et al.*, Nucl. Phys. A **504** (1989) 205-230.
- [18] D. Rudolph, priv. comm..
- [19] D. Rudolph, priv. comm..
- [20] C. E. Svensson *et al.*, Phys. Rev. Lett. **82** (1999) 3400-3403.
- [21] D. Rudolph, priv. comm..